Article

Energetics and Structural Consequences of Axial Ligand Coordination in Nonplanar Nickel Porphyrins

Yujiang Song, Raid E. Haddad, Song-Ling Jia, Saphon Hok, Marilyn M. Olmstead,
Daniel J. Nurco, Neal E. Schore, Jun Zhang, Jian-Guo Ma, Kevin M. Smith, Stphanie
Gazeau, Jacques Pcaut, Jean-Claude Marchon, Craig J. Medforth, and John A. Shelnutt

J. Am. Chem. Soc., **2005**, 127 (4), 1179-1192• DOI: 10.1021/ja045309n • Publication Date (Web): 07 January 2005

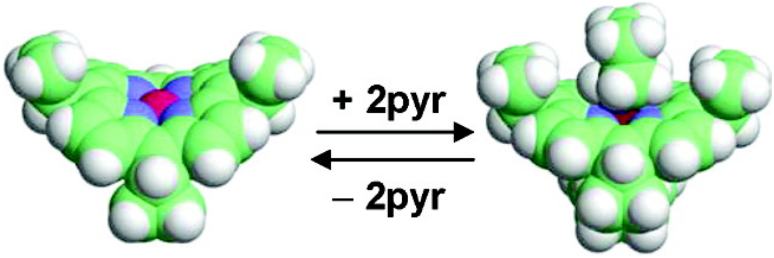

Journal of the American Chemical Society is published by the American Chemical Society. 1155 Sixteenth Street N.W., Washington, DC 20036

J|A|C|S
ARTICLES

Energetics and Structural Consequences of Axial Ligand Coordination in Nonplanar Nickel Porphyrins

Yujiang Song,[†,‡] Raid E. Haddad,[†,‡] Song-Ling Jia,[†,‡] Saphon Hok,[§]
Marilyn M. Olmstead,[§] Daniel J. Nurco,[§] Neal E. Schore,[§] Jun Zhang,[†,‡]
Jian-Guo Ma,[†,‡] Kevin M. Smith,[∥] Stéphanie Gazeau,[⊥] Jacques Pécaut,[⊥]
Jean-Claude Marchon,[⊥] Craig J. Medforth,*[,†,§] and John A. Shelnutt*[,†,#]

Contribution from the Biomolecular Materials and Interfaces Department, Sandia National Laboratories, Albuquerque, New Mexico 87185; Departments of Chemistry and Chemical and Nuclear Engineering, University of New Mexico, Albuquerque, New Mexico 87131; Department of Chemistry, University of California, Davis, California 95646; Department of Chemistry, Louisiana State University, Baton Rouge, Louisiana 70803; Laboratoire de Chimie Inorganique et Biologique, Département de Recherche Fondamentale sur la Matière Condensée, CEA-Grenoble, 38054 Grenoble, France; and Department of Chemistry, University of Georgia, Athens, Georgia 30602

Received August 3, 2004; E-mail: jasheln@unm.edu

Abstract: The effects of ruffling on the axial ligation properties of a series of nickel(II) tetra(alkyl)porphyrins have been investigated with UV−visible absorption spectroscopy, resonance Raman spectroscopy, X-ray crystallography, classical molecular mechanics calculations, and normal-coordinate structural decomposition analysis. For the modestly nonplanar porphyrins, porphyrin ruffling is found to cause a decrease in binding affinity for pyrrolidine and piperidine, mainly caused by a decrease in the binding constant for addition of the first axial ligand; ligand binding is completely inhibited for the more nonplanar porphyrins. The lowered affinity, resulting from the large energies required to expand the core and flatten the porphyrin to accommodate the large high-spin nickel(II) ion, has implications for nickel porphyrin-based molecular devices and the function of heme proteins and methyl-coenzyme M reductase.

Introduction

Nickel tetrapyrroles occur in biology as cofactor F430 of the enzyme methyl-coenzyme M reductase,[1,2] which catalyzes methane formation from methyl-coenzyme M and *N*-7-mercaptoheptanoylthreonine phosphate, and as tunichlorins in tunicates and mollusks.[3] Cofactor F430, a reduced nickel hydrocorphin containing Ni(I) in its active form,[4] has recently been investigated in the native enzyme,[5] and the results were compared with previous[6−9] and new data[5] on the inactive Ni(II) EPR-silent forms. F430 is axially coordinated in all protein-bound forms. Studies of the Ni(II) species showed that there is an additional conformational change in F430 upon binding to the protein, a conformational difference which persists for the active reduced Ni(I) form of the enzyme.[5] Axial ligand exchange occurs in the protein when the nickel oxidation state changes and during the catalytic reaction. Given the limited number of studies of the relationship between tetrapyrrole nonplanarity and axial ligand affinity, we decided to systematically investigate the relationship between tetrapyrrole conformation and axial ligand affinity using a series of nickel porphyrins with increasingly nonplanar macrocycles generated by more bulky *meso* alkyl substituents. An additional reason for this study was to investigate the possibility that the change from low-spin nickel(II) to the larger high-spin nickel(II) might be exploited in the design of chemically or optically switched porphyrin-based molecular mechanical devices (e.g., nanotweezers).[10]

The structures, spectroscopic properties, and chemical behavior of nickel tetrapyrroles have been extensively investigated using a range of experimental and theoretical techniques. Low-spin nickel(II) porphyrins have been the most widely studied nickel tetrapyrroles; Ni(II) has a $(d_{z^2})^2$ electronic configuration and favors relatively short equilibrium Ni−N bond distances, resulting in a tendency for the porphyrin macrocycle to adopt

---

[†] Sandia National Laboratories.

[‡] University of New Mexico.

[§] University of California.

[∥] Louisiana State University.

[⊥] CEA-Grenoble.

[#] University of Georgia.

(1) Taylor, C. D.; Wolfe, R. S. *J. Biol. Chem.* **1974**, *249*, 4879−4885.

(2) Gunsalus, R. P.; Wolfe, R. S. *Biochem. Biophys. Res. Commun.* **1977**, *76*, 790−795.

(3) Bible, K. C.; Buytendorp, M.; Zierath, P. D.; Rinehard, K. L. *Proc. Natl. Acad. Sci. U.S.A.* **1988**, *85*, 4582−4586.

(4) Rouviere, P. E.; Bobik, T. A.; Wolfe, R. S. *J. Bacteriol.* **1988**, *170*, 3946−3952.

(5) Tang, Q.; Carrington, P. E.; Horng, Y.-C.; Maroney, M. J.; Ragsdale, S. W.; Bocian, D. F. *J. Am. Chem. Soc.* **2002**, *124*, 13242−13256.

(6) Shiemke, A. K.; Hamilton, C. L.; Scott, R. A. *J. Biol. Chem.* **1988**, *263*, 5611−5616.

(7) Shiemke, A. K.; Scott, R. A.; Shelnutt, J. A. *J. Am. Chem. Soc.* **1988**, *110*, 1645−1646.

(8) Shiemke, A. K.; Kaplan, W. A.; Hamilton, C. L.; Shelnutt, J. A.; Scott, R. A. *J. Biol. Chem.* **1989**, *264*, 7276−7284.

(9) Shiemke, A. K.; Shelnutt, J. A.; Scott, R. A. *J. Biol. Chem.* **1989**, *264*, 11236−11245.

(10) Gazeau, S.; Pécaut, J.; Marchon, J. C. *Chem. Commun.* **2001**, 1644−1645.

10.1021/ja045309n CCC: $30.25 © 2005 American Chemical Society

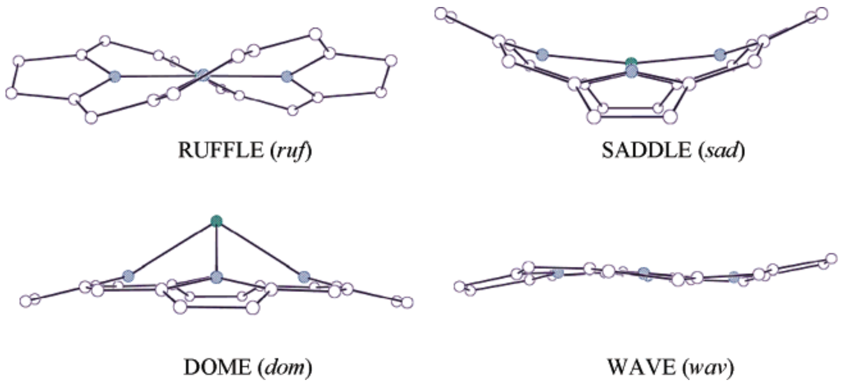

Figure 1. Representations of the lowest-energy nonplanar deformation modes of the porphyrin macrocycle[17] that are commonly observed in porphyrin crystal structures.

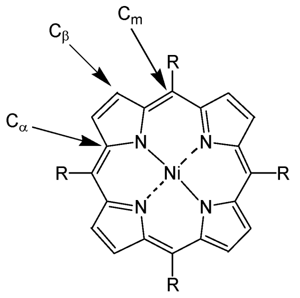

NiT(Me)P R = methyl

NiT(Et)P R = ethyl
NiT(Pr)P R = propyl
NiT(Pe)P R = pentyl

NiT(iPr)P R = iso-propyl
NiT(cH)P R = cyclohexyl
NiT(cPr)P R = cyclopropyl

NiT(tBu)P R = tert-butyl

Figure 2. Structures of the nickel(II) tetra(alkyl) porphyrins discussed in this study.

a nonplanar conformation (e.g., the ruffled structure shown in Figure 1).[11−13] High-spin nickel(II) porphyrins with (d_{z^2})-$(d_{x^2-y^2})$ electronic states have been obtained by axial ligation or by photoexcitation to a Ni d,d excited state. In axially ligated high-spin nickel porphyrins, the equilibrium Ni−N bond distance is elongated by ~0.2 Å because of the presence of an electron in the antibonding $d_{x^2-y^2}$ orbital, and the Ni−N distance in the porphyrin expands to approximate that seen for zinc(II) or Ni(I) complexes. Switching from low-spin to high-spin nickel can induce a considerable change in the conformation of the porphyrin ring, by flattening the macrocycle and/or changing to another type of nonplanar conformation which more readily accommodates the larger high-spin nickel (e.g., a dome structure).[14−17]

In this paper, we investigate axial ligand binding in the series of nickel(II) tetra(alkyl)porphyrins shown in Figure 2, for which nonplanar deformations of the macrocycle (primarily ruffling) are induced by steric forces arising from the alkyl substituents at the *meso* positions.[18] Previous crystallographic and spectroscopic studies have shown that larger alkyl substituents give more nonplanar macrocycles,[18,19] thus providing a series of compounds for which the amount of nonplanar deformation varies while the substituent electronic effect stays nearly constant. The goals of the current study are to structurally and spectroscopically characterize the unligated and ligated forms of these nickel(II) tetra(alkyl)porphyrins, to determine the effect of varying degrees of substituent induced nonplanarity on axial ligand affinity, and to quantify the structural consequences of ligand binding and especially the potential for ligand-induced switching between stable conformers.

Initially, the low-spin four-coordinate forms of the nickel(II) tetra(alkyl)porphyrins are characterized. X-ray crystallographic studies are reported, with three new crystal structures including the newly synthesized cyclopropyl derivative. The conformational landscapes of the nickel tetra(alkyl)porphyrins are then investigated using molecular mechanics (MM) calculations.[13,20,21] Both the X-ray and MM structures are analyzed using normal-coordinate structural decomposition (NSD),[13,17,22,23] a technique developed for characterizing nonplanar distortions of porphyrins that has been used extensively to investigate the deformations of heme groups in proteins[13,22,24] and in isolated tetrapyrroles.[13,20,25] In section II, UV−visible absorption and resonance Raman (RR) spectroscopy are employed to characterize the nickel(II) tetra(alkyl)porphyrins in both noncoordinating (dichloromethane, carbon disulfide, benzene) and strongly coordinating (pyrrolidine, piperidine) solvents to determine the effect of nonplanarity on axial ligand affinity. The effect of the macrocycle conformation on the ligand binding energy and the effect of axial ligation on the porphyrin conformational energy landscape are investigated in section III. Finally, potential uses of the small but energetically significant structural change at the nickel ion to drive molecular nanomachines (e.g., nanotweezers) and the possible significance of the results obtained for the function of methyl-coenzyme M reductase and heme proteins are discussed.

---

(11) Hoard, J. L. In *Porphyrins and Metalloporphyrins*; Smith, K. M., Ed.; Elsevier: Amsterdam, 1975; pp 317−380.
(12) Sparks, L. D.; Medforth, C. J.; Park, M. S.; Chamberlain, J. R.; Ondrias, M. R.; Senge, M. O.; Smith, K. M.; Shelnutt, J. A. *J. Am. Chem. Soc.* **1993**, *115*, 581−592.
(13) Shelnutt, J. A. In *The Porphyrin Handbook*; Kadish, K. M., Smith, K. M., Guilard, R., Eds.; Academic Press: New York, 2000; Vol. 7, pp 167−223.
(14) Jia, S.-L.; Jentzen, W.; Shang, M.; Song, X.-Z.; Ma, J.-G.; Scheidt, W. R.; Shelnutt, J. A. *Inorg. Chem.* **1998**, *37*, 4402−4412.
(15) Senge, M. O. *J. Porphyrins Phthalocyanines* **1998**, *2*, 107−121.
(16) Duval, H.; Bulach, V.; Fischer, J.; Weiss, R. *Inorg. Chem.* **1999**, *38*, 5495−5501.
(17) Jentzen, W.; Song, X. Z.; Shelnutt, J. A. *J. Phys. Chem. B* **1997**, *101*, 1684−1699.
(18) Jentzen, W.; Simpson, M. C.; Hobbs, J. D.; Song, X.; Ema, T.; Nelson, N. Y.; Medforth, C. J.; Smith, K. M.; Veyrat, M.; Mazzanti, M.; Ramasseul, R.; Marchon, J. C.; Takeuchi, T.; Goddard, W. A., III.; Shelnutt, J. A. *J. Am. Chem. Soc.* **1995**, *117*, 11085−11097.
(19) Haddad, R.; Gazeau, S.; Pécaut, J.; Marchon, J. C.; Medforth, C. J.; Shelnutt, J. A. *J. Am. Chem. Soc.* **2003**, *125*, 1253−1268.
(20) Song, X. Z.; Jaquinod, L.; Jentzen, W.; Nurco, D. J.; Jia, S. L.; Khoury, R. G.; Ma, J. G.; Medforth, C. J.; Smith, K. M.; Shelnutt, J. A. *Inorg. Chem.* **1998**, *37*, 2009−2019.
(21) Shelnutt, J. A.; Medforth, C. J.; Berber, M. D.; Barkigia, K. M.; Smith, K. M. *J. Am. Chem. Soc.* **1991**, *113*, 4077−4087.
(22) Jentzen, W.; Ma, J. G.; Shelnutt, J. A. *Biophys. J.* **1998**, *74*, 753−63.
(23) Shelnutt, J. A.; Song, X. Z.; Ma, J. G.; Jia, S. L.; Jentzen, W.; Medforth, C. J. *Chem. Soc. Rev.* **1998**, *27*, 31−41.
(24) Hobbs, J. D.; Shelnutt, J. A. *J. Protein Chem.* **1995**, *14*, 19−25.
(25) Song, X. Z.; Jentzen, W.; Jaquinod, L.; Khoury, R. G.; Medforth, C. J.; Jia, S. L.; Ma, J. G.; Smith, K. M.; Shelnutt, J. A. *Inorg. Chem.* **1998**, *37*, 2117−2128.

Materials and Methods

Materials. NiTPP was obtained from Porphyrin Products (Logan, UT) and used without further purification. The syntheses of NiT(Me)P, NiT(Et)P, NiT(Pr)P, NiT(Pe)P, NiT(*i*Pr)P, NiT(cH)P, and NiT(*t*Bu)P have been given elsewhere.[18] The synthesis of NiT(cPr)P is described below. Benzene, dichloromethane, piperidine, pyrrolidine, and 2,3-dichloro-5,6-dicyano-1,4-benzoquinone (DDQ) were of the highest purity available from Aldrich (St. Louis) and were used as received.

A. Synthesis of Nickel(II) 5,10,15,20-Tetra(cyclopropyl)porphyrin (NiT(cPr)P): Freshly distilled dichloromethane (1000 mL), freshly distilled pyrrole (4.85 mL, 0.07 mol), and cyclopropane carboxaldehyde (5.0 g, 0.07 mol) (98%, Aldrich) were added to a dried three-necked 2-L round-bottomed flask. The solution was stirred under argon for 30 min at room temperature, $BF_3{\cdot}OEt_2$ (1.45 mL, 0.07 mol) was added dropwise via syringe, and the reaction stirred at room temperature in the dark for 17 h. DDQ (11.30 g, 0.07 mol) was added, and the reaction mixture refluxed for 1 h. It was then cooled to room temperature, the polymeric materials were filtered off, and the filtrate was poured through a plug of Grade III alumina and washed with dichloromethane (500 mL). The combined filtrates were concentrated and chromatographed on a Grade III alumina column eluted with dichloromethane/cyclohexane (50/50, v/v). The greenish yellow band was collected, the eluent was removed by evaporation, and the resulting solid residue was recrystallized from dichloromethane by adding cyclohexane to afford H_2T(cPr)P as a purple powder (0.64 g, 7.8% yield). ^1H NMR ($CDCl_3$): δ −2.39 (br s, 2H, NH), 1.43 and 1.82 (m, 8H each, $-CH_2-$), 4.21 (m, 4H, $-CH-$), 9.73 (s, 8H, β-H). UV/vis (CH_2Cl_2) λ_{max}, nm ($\epsilon \times 10^{-3}$): 423 (333), 522 (13.5), 559 (5.4), 604 (4.2), 660 (2.2). To prepare NiT(cPr)P, H_2T(cPr)P (200 mg, 0.43 mmol) was dissolved in dichloromethane (180 mL), the solution was brought to reflux, and a saturated solution of nickel(II) acetate in methanol (25 mL) was added. Refluxing was continued under argon for 17 h. The reaction mixture was then cooled to room temperature, washed with water (3 × 500 mL) and brine (500 mL), and dried over anhydrous magnesium sulfate. After filtration, the filtrate was concentrated to about 5 mL and treated with methanol (20 mL) to produce shiny purple/red crystals of NiT(cPr)P (193 mg, 86%). ^1H NMR ($CDCl_3$): δ 0.81 and 1.49 (m, 8H each, $-CH_2-$), 4.05 (m, 4H, $-CH-$), 9.47 (s, 8H, β-H). UV/vis (CH_2Cl_2) λ_{max}, nm ($\epsilon \times 10^{-3}$): 423 (201), 544 (13.5), 582 (2.7).

X-ray Crystallography. Published crystal structures were taken from the January 2004 release of the Cambridge Structure Database.

A. NiT(cPr)P. Crystals were grown by slow diffusion of methanol into a solution of NiT(cPr)P in dichloromethane. A red block was mounted in the 90(2) K nitrogen cold stream provided by a CRYO Industries low-temperature apparatus on the goniometer head of a Bruker SMART 1000 diffractometer. Diffraction data were collected with graphite-monochromated Mo Kα radiation employing a 0.3° ω scan and approximately a full sphere of data to a $2\theta_{max}$ of 63°. Data collection was performed with SMART,[26] data integration was performed with SAINT,[27] and a multiscan correction for absorption was applied using the program SADABS.[28] A total of 6447 reflections were obtained after truncation to a 2θ of 46.5°, of which 1766 were unique (R(int) = 0.038) and 1732 were observed ($I > 2\sigma(I)$). The structure was solved by direct methods (SHELXS97) and refined by full-matrix least-squares on F^2 (SHELXL97).[29] The maximum and minimum peaks in the final difference Fourier map corresponded to 0.29 and −0.16 $eÅ^{-3}$, respectively. The absolute structure was determined; Flack parameter 0.013(13).[30]

B. NiT(Pe)P (Polymorph 1). Crystals were grown by slow diffusion of methanol into a solution of NiT(Pe)P in dichloromethane. A red needle was mounted on the goniometer head of the Bruker SMART diffractometer and processed in the manner described above. A total of 60 270 reflections were obtained after truncation to a 2θ of 50.7°, of which 23 791 were unique (R(int) = 0.037) and 13 916 were observed ($I > 2\sigma(I)$). The structure has four molecules in the asymmetric unit. Each differs in the conformation of the *n*-pentyl groups and in their disorder. Only the fourth molecule (Ni4) has no disorder in the alkyl chains. The porphyrin containing Ni1 has disorder (50:50) in (C23A, C24A, C25A):(C23B, C24B, C25B). The porphyrin containing Ni2 has disorder (50:50) in (C66A, C67A, C68A):(C66B, C67B, C68B) and (C71A, C72A, C73A, C74A, C75A):(C71B, C72B, C73B, C74B, C75B). The porphyrin containing Ni3 has disorder (50:50) in (C117, C118):(C17B, C18B) and (C102, C103, C104, C105):(C12B, C13B, C14B, C15B) and (C113, C114):(C311, C411). The maximum and minimum peaks in the final difference Fourier map corresponded to 0.70 and −1.45 $eÅ^{-3}$, respectively.

C. NiT(Pe)P (Polymorph II). The second polymorph of NiT(Pe)P was obtained as red-brown needles by slow evaporation from a solution in piperidine. A total of 15 674 reflections were obained after truncation to a 2θ of 50.7°, of which 6134 were unique (R(int) = 0.081) and 3716 were observed ($I > 2\sigma(I)$). In contrast to polymorph I, there is only one molecule in the asymmetric unit, but there is similar disorder in the pentyl groups. There is 50:50 disorder in (C25):(C25B), (C32, C33):(C32B, C33B), and (C37, C38, C39, C40):(C37B, C38B, C39B, C40B). There is 75:25 disorder in the groups (C27, C28, C29, C30):(C27B, C28B, C29B, C30B). The maximum and minimum peaks in the final difference Fourier map corresponded to 0.79 and −0.74 $eÅ^{-3}$, respectively.

D. NiT(Pr)P. Previously, the X-ray crystal structure of NiT(Pr)P and XAFS studies have been reported briefly.[31] The crystal growth and structure refinement for another NiT(Pr)P crystal are reported here briefly and will be reported in detail elsewhere.

UV−visible Absorption Spectroscopy. UV−visible spectra were obtained using an HP 8452A diode array spectrophotometer (Colorado Springs, CO) and a 5-mm path length quartz cell. The absorption spectra were measured in dichloromethane (Figure 4), pyrrolidine (Figure 5), or piperidine (Figure 6). The peak positions were obtained by curve-fitting the absorption spectra with Gaussian lines using the program PeakFit (SSPS, Richmond, CA).

A typical procedure for the photometric titrations is illustrated using NiT(Pr)P as an example. NiT(Pr)P stock solution (43.7 μM) was prepared by dissolving the nickel porphyrin complex in benzene. The solution was sonicated for 30 min and left overnight in the dark at room temperature to ensure that of all the porphyrin was dissolved. Porphyrin stock solution (300 μL) was diluted with mixtures of benzene and pyrrolidine (2 mL) and added to a 1-cm quartz cuvette. The final porphyrin concentration was 5.7 μM. For solutions containing low concentrations of pyrrolidine in benzene, a single sample was made by diluting porphyrin stock solution (300 μL) in benzene (2 mL). Using this solution, the concentration of pyrrolidine was progressively increased by adding thirteen 2-μL, five 5-μL, four 10-μL, and three 20-μL aliquots of pyrrolidine with a glass syringe. The dilution effect caused by the added pyrrolidine was ignored when fitting the photometric titrations. Optical spectra obtained from a typical titration are shown in Figure S2.

The change in absorbance at the absorption maxima of the ligated species was fitted using the equilibrium constants K_1 and K_2 and with a single equilibrium constant β (see Scheme 1). The equations and approximations used to fit the change in absorbance with the consecutive equilibria K_1 and K_2 are described in Text S1 of the Supporting Information. The estimated errors in the values of K_1 and K_2 determined

---

(26) Data collection: *SMART*, v. 5.054; Bruker Analytical X-ray Instruments: Madison, WI, 2002.

(27) Data reduction: *SAINT*, v. 6.36A.; Bruker Analytical X-ray Instruments: Madison, WI, 2002.

(28) Sheldrick, G. M. *SADABS 2.10*; University of Göttingen: Germany, 2003.

(29) Sheldrick, G. M. *SHELXTL*, v. 5.10; Bruker Analytical X-ray Instruments: Madison, WI, 1997.

(30) Flack, H. D. *Acta Crystallogr.* **1983**, *A39*, 876−881.

(31) Renner, M. W.; Furenlid, L. R.; Barkigia, K. M.; Fajer, J. *J. Phys. IV* **1997**, *7*, 661−662.

Scheme 1. Definition of the Equilibrium Constants for Ligation of the Nickel Tetra(alkyl)Porphyrins

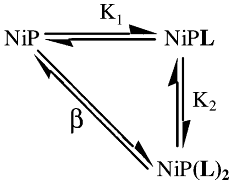

using this method are typically 25%. Curve-fitting the absorbance data using the equation derived for β (see Text S1) results in estimated errors of less than 5%. The larger errors obtained for K_1 and K_2 compared to β are consistent with K_1 and K_2 being correlated, although under any reasonable scenario K_1 is orders of magnitude smaller than K_2. The curve fits obtained for NiTPeP and NiTPrP using the single equilibrium constant β are shown in Figure S3.

Resonance Raman Spectroscopy. Resonance Raman (RR) spectra of porphyrin solutions were obtained using a partitioned quartz cell and a dual-channel spectrometer[33] or a CCD spectrometer[34] described previously. The scattered light was collected at 90° to the directions of propagation and polarization of the exciting laser beam. The partitioned cylindrical Raman cell was rotated at 50 Hz to avoid local heating and to probe alternately the sample and reference solutions. The typical conditions were 50−60 mw of laser power, 5-cm^{-1} spectral slit width, 8−10 scans with 0.3-cm^{-1} step increments, and 0.5-s integration times on individual scans for the dual-channel spectrometer. The spectra from the dual-channel spectrometer were corrected for the nonlinear response of the spectrometer and PMT detector. For the spectra obtained with the CCD spectrometer, low power ($<$20 mW) was used with a 3 × 3-mm^2 cross section quartz cell at room temperature. The 413.1-nm line of a Coherent INNOVA krypton ion laser (Santa Clara, CA) was used as the excitation source, and NiTPP in neat benzene was employed as the reference solution for the Raman line frequencies. For the CCD spectrometer, the spectra were obtained in 10 min or less. Polarized spectra were measured by passing the scattered light through a Polaroid sheet oriented parallel or perpendicular to the polarization direction of the incident beam, followed by a polarization scrambler in front of the spectrometer entrance slit.

Molecular Mechanics Calculations. MM calculations were performed using a force field developed[21] and refined[20] by Shelnutt and co-workers. The calculations were carried out using Cerius^2 software from Accelrys (San Diego) on a Silicon Graphics Octane workstation. The force field used in the calculations is based on DREIDING II, modified to include force constants and equilibrium values for bond lengths, bond angles, torsion angles, and improper torsion (umbrella) angles of the porphyrin macrocycle, as well as parameters describing the van der Waals and electrostatic interactions for the porphyrin macrocycle.[21] The force field has been used extensively to calculate the structures of porphyrins[13] and to investigate some dynamic processes such as axial ligand rotation[35,36] and substituent rotation.[37]

For the high-spin four-coordinate and high-spin axially ligated (five- and six-coordinate) nickel complexes, an equilibrium Ni−N$_{\text{pyrrole}}$ bond length of 2.07 Å was used in the calculations. This value was obtained by varying the equilibrium Ni−N$_{\text{pyrrole}}$ bond length in the energy-optimized structure of nickel(II) tetra(*N*-methyl-pyridinium)porphyrin bis-imidazole until the calculated structure best matched the crystal structure.[14,38] The force constant for the Ni−N$_{\text{ligand}}$ bond was taken to be the same as for the low-spin Ni−N$_{\text{pyrrole}}$ bond. Note that the Ni−N$_{\text{pyrrole}}$ bond length of 2.07 Å is the same as that used for zinc(II).[12] The N$_{\text{pyrrole}}$−Ni−N$_{\text{ligand}}$ angle was modeled using default parameters, with a θ-harmonic potential, a minimum at 90°, and a force constant of 100. The van der Waals parameters for high-spin and axially ligated nickel have little effect on the structure and were approximated using the value for zinc(II) in the DREIDING II force field.[39] The torsion angle force constant for rotation about the Ni−N$_{\text{ligand}}$ bond was set to zero. For consistency with earlier studies, a dielectric constant of 2.64 (for carbon disulfide) was used in the calculations. Energy optimization calculations were performed from different starting structures (e.g., $\alpha\beta\alpha\beta$, $\alpha\alpha\alpha\beta$, $\alpha\alpha\beta\beta$, and $\alpha\alpha\alpha\alpha$ conformers, and additional orientations for the asymmetric alkyl groups) to search for the stable conformations of the nickel tetra(alkyl)porphyrins.

Normal-Coordinate Structural Decomposition. Normal-coordinate structural decomposition (NSD)[13,17] is used to analyze the out-of-plane (and in-plane) deformations present in the porphyrin crystallographic and MM structures. The NSD method characterizes the porphyrin conformation in terms of equivalent displacements along the normal coordinates of the D_{4h}-symmetric porphyrin macrocycle. Typically, the largest static distortions of the porphyrin macrocycle occur along the softest normal modes, so that the greatest contributors to the nonplanar distortion are the lowest-frequency normal coordinates of each out-of-plane symmetry type (B_{1u}, B_{2u}, A_{2u}, E_g, and A_{1u}). These deformations correspond to the symmetric distortions commonly observed in crystal structures and are named ruffling (*ruf*), saddling (*sad*), doming (*dom*), waving (*wav*(*x*,*y*)), and propellering (*pro*) (see Figure 1 for illustrations of the *ruf*, *sad*, *dom*, and *wav* deformations). Mixed together, they give asymmetric macrocyclic distortions of various types, and (vectorially) adding the projections of the total distortion along only these six normal coordinates typically simulates the actual out-of-plane distortion reasonably accurately. In the present study, only the deformations for these lowest-frequency normal modes are discussed. Note that although the contributions to the distortion from the high-frequency modes are small, they have important consequences for the optical spectra[19] and possibly other properties of tetrapyrroles. (The signs of the deformations have been omitted in this work as they are dependent on the way the molecule is oriented for the NSD analysis.) A browser based version of the NSD program is available for public use at http://jasheln.unm.edu.

Results and Discussion

I. Structures of the Low-Spin Nickel(II) Tetra(alkyl)porphyrins. A. X-ray Crystallography. The nickel(II) tetra(alkyl)porphyrins used in the present study provide a series of compounds with similar substituent electronic effects but with varying degrees of ruffling due to differences in the steric bulk of the substituents. This provides a practical way to investigate the effects of porphyrin macrocycle nonplanarity on axial ligand affinity without significant interference from substituent electronic effects. The nickel(II) porphyrins can be divided into four classes according to whether the alkyl substituent is a methyl group or a primary, secondary, or tertiary alkyl group. Three new crystal structures, NiT(Pr)P, NiT(Pe)P, and NiT(cPr)P, are shown in Figure 3. Selected structural parameters for these compounds and for previously published compounds of this class of porphyrin are given in Table 1. Details of the NSD analyses are provided in Table 2, and full output files from the NSD analyses are given in Table S1.

---

(32) Ulman, A.; Gallucci, J.; Fisher, D.; Ibers, J. A. *J. Am. Chem. Soc.* **1980**, *102*, 6852.
(33) Shelnutt, J. A. *J. Phys. Chem.* **1983**, *87*, 605−616.
(34) Franco, R.; Ma, J.-G.; Lu, Y.; Ferreira, G. C.; Shelnutt, J. A. *Biochemistry* **2000**, *39*, 2517−2529.
(35) Medforth, C. J.; Muzzi, C. M.; Smith, K. M.; Abraham, R. J.; Hobbs, J. D.; Shelnutt, J. A. *J. Chem. Soc., Chem. Commun.* **1994**, 1843−1844.
(36) Medforth, C. J.; Muzzi, C. M.; Shea, K. M.; Smith, K. M.; Abraham, R. J.; Jia, S. L.; Shelnutt, J. A. *J. Chem. Soc., Perkin Trans. 2* **1997**, 833−837.
(37) Medforth, C. J.; Haddad, R.; Muzzi, C. M.; Dooley, N. R.; Jaquinod, L.; Shyr, D. C.; Nurco, D. J.; Olmstead, M. M.; Smith, K. M.; Ma, J. G.; Shelnutt, J. A. *Inorg. Chem.* **2003**, *42*, 2227−2241.
(38) Ma, J.-G., Vanderkooi, J. M.; Zhang, J.; Jia, S.-L.; Shelnutt, J. A. *Biochemistry* **1999**, *38*, 2787−2795.
(39) Mayo, S. L.; Olafson, B. D.; Goddard, W. A. *J. Phys. Chem.* **1990**, *94*, 8897−8909.

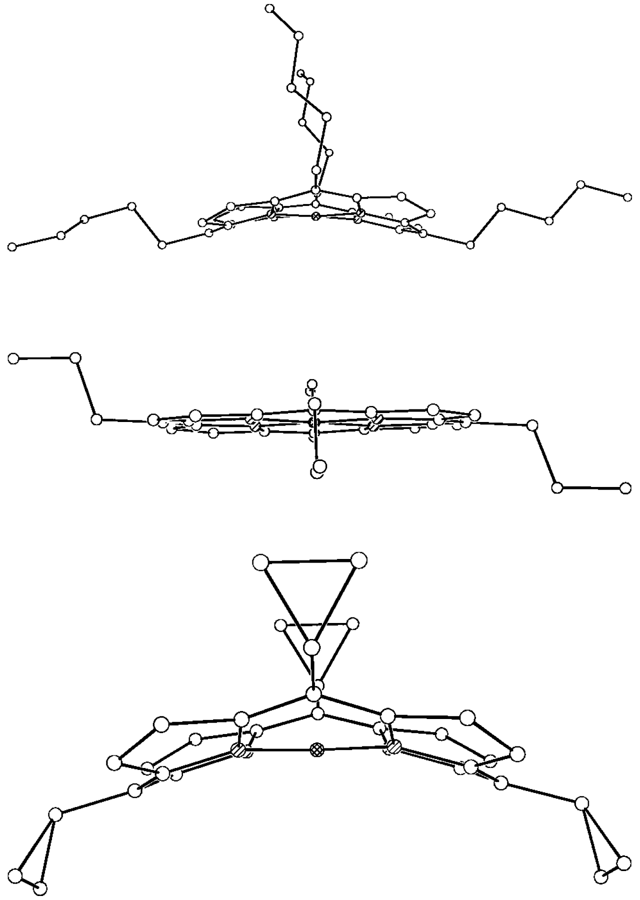

Figure 3. Crystal structures of NiT(Pe)P (upper), NiT(Pr)P (middle), and NiT(cPr)P (lower).

The Ni−N distance is a measure of the contraction of the porphyrin core, and it decreases as the porphyrin becomes more ruffled (Table 1). The C_α−N−N−C_α torsion angle (or ruffling angle) measures the extent to which the planes of opposing pyrrole rings are twisted by ruffling of the porphyrin ring and increases as the amount of deformation increases. The N−C_α−C_m−C_α torsion angle (or π-overlap angle) characterizes the degree of π-overlap between the pyrrole rings. It has been shown to correlate well with spectroscopic markers of porphyrin nonplanarity (e.g., red shifting of UV−visible absorption bands).[19]

The new structures of NiT(Pr)P and NiT(Pe)P (Figure 3) demonstrate the importance of crystal packing forces in determining the porphyrin conformation. NSD analyses of the structures show that NiT(Pr)P is almost planar (d_{obs} = 0.173 Å, d_{ruf} = 0.001 Å), whereas the similar porphyrin NiT(Pe)P is ruffled (d_{ruf} = 1.572 Å). Interestingly, the NSD analyses (Table 2) show that the almost planar crystal structures of NiT(Pr)P and NiT(Me)P actually contain waving deformations that, although small, correspond to considerable amounts of deformation energy.[18,45] The structures of NiT(Me)P and NiT(Pr)P also show a long metal−nitrogen distance which is not optimal for coordination to low-spin nickel(II) (Table 1). Taken together, these results suggest that the crystal structures seen for NiT(Pr)P and NiT(Me)P are the result of favorable crystal packing interactions but nonoptimum macrocycle conformations. Crystal packing influences are known to result in both ruffled and planar crystalline forms of the reference compound NiOEP. Similar conclusions regarding macrocycle flexibility were obtained from previous X-ray crystal structures and XAFS studies of NiT(Pr)P,[31] which found that the Ni−N distance in solution was much shorter than that in the crystal indicating a nonplanar macrocycle in solution. The MM calculations reported here, which give only small energy differences between a nearly planar structure and the ruffled structure (see below), are consistent with this interpretation.

Table 1. Selected Structural Parameters from Four-Coordinate Nickel(II) Tetra(alkyl)porphyrin X-ray Crystal Structures

porphyrin	Ni–N (Å)	C_α–N–N–C_α (deg) (ruffling angle)	N–C_α–C_m–C_α (deg) (π-overlap angle)
NiT(Me)P[32] (TCLNIB01)	1.953	0.9	3.6
Primary Alkyl Groups			
NiT(Pe)P (this work)[a]	1.922	34.1	8.0
NiT(Pe)P (this work)[b]	1.925	33.2	8.6
NiT(Pr)P (this work)[40]	1.963	1.0	1.9
NiT(2-Me-Pr)P[41] (DOWCAT)[c]	1.908	40.3	10.3
Secondary Alkyl Groups			
NiT(cPr)P (this work)	1.902	44.6	12.1
NiT(*i*Pr)P[42] (HETDAL)	1.896	43.7	12.6
NiT(cH)P[43] (ZULMOI)	1.888	46.2	13.8
NiT(1-Et-Pr)[41] (DOWDUO)	1.889	49.0	13.2
Tertiary Alkyl Groups			
NiT(*t*Bu)P[44]	1.869	n/a	n/a
Reference Compounds			
NiP	1.951	1.6	0.8
NiTPP	1.931	27.3	7.5
NiOEP triclinic A	1.958	1.4	0.7
NiOEP triclinic B	1.952	0.8	2.1
NiOEP tetragonal	1.930	31.9	7.8

[a] Data are taken from the structure of NiT(Pe)P crystallized from dichloromethane by slow diffusion of methanol. Structural parameters are for one of four molecules with similar macrocycle conformations (molecule analyzed contains Ni4 and has the least disorder of the pentyl groups). [b] Data are taken from the structure of NiT(Pe)P crystallized by slow evaporation of a solution in piperidine. [c] Data are for one of two molecules with similar macrocycle conformations (molecule analyzed contains Ni1).

The conformational heterogeneity and influence of crystal packing forces apparent for the porphyrins with primary alkyl substituents are not seen for the porphyrins which have the bulkier secondary alkyl substituents (cPr, *i*Pr, cH, 1-Et-Pr). All four crystal structures are very ruffled (d_{obs} 2.07−2.26 Å), have short Ni−N distances (1.888−1.902 Å), large ruffling angles (43.7°−49.0°), and large π-overlap angles (12.1°−13.8°) (Table 1). Only a limited amount of structural data are available for the tertiary alkyl-substituted porphyrin NiT(*t*Bu)P, but the short Ni−N distance confirms that it is more nonplanar than the nickel porphyrins with secondary alkyl substituents.

B. Molecular Mechanics Calculations. The MM studies show that the porphyrins typically have four distinct stable conformers resulting from different positions of the peripheral alkyl substituents relative to the porphyrin mean plane ($\alpha\beta\alpha\beta$,

---

(40) Nurco, D. J. Personal communication.

(41) Senge, M. O.; Bischoff, I.; Nelson, N. Y.; Smith, K. M. *J. Porphyrins Phthalocyanines* **1999**, *3*, 99−116.

(42) Ema, T.; Senge, M. O.; Nelson, N. Y.; Ogoshi, H.; Smith, K. M. *Angew. Chem., Int. Ed. Engl.* **1994**, *33*, 1879−1881.

(43) Veyrat, M.; Ramasseul, R.; Marchon, J. C.; Turowskatyrk, I.; Scheidt, W. R. *New J. Chem.* **1995**, *19*, 1199−1202.

(44) Drain, C. M.; Gentemann, S.; Roberts, J. A.; Nelson, N. Y.; Medforth, C. J.; Jia, S. L.; Simpson, M. C.; Smith, K. M.; Fajer, J.; Shelnutt, J. A.; Holten, D. *J. Am. Chem. Soc.* **1998**, *120*, 3781−3791.

(45) Jentzen, W.; Song, X.; Shelnutt, J. A. *Biophys. J.* **1996**, *70*, A153−A153.

Table 2. Out-of-Plane Displacements (in Å) for the Crystal Structures of the Four-Coordinate Low-Spin Nickel(II) Tetra(alkyl)porphyrins from Normal-Coordinate Structural Decomposition

	total distortion		B_{2u}[c]	B_{1u}	A_{2u}	$E_g(x)$	$E_g(y)$	A_{1u}
porphyrin	d_{obs}[a]	d_{calc}[b]	d_{sad}	d_{ruf}	d_{dom}	$d_{\text{wav}(x)}$	$d_{\text{wav}(y)}$	d_{pro}
NiT(Me)P	0.296	0.273	0.000	0.000	0.001	0.268	0.050	0.000
NiT(Pe)P[d]	1.644	1.643	0.462	1.572	0.106	0.055	0.041	0.013
NiT(Pe)P[e]	1.657	1.656	0.572	1.552	0.067	0.056	0.040	0.007
NiT(Pr)P	0.173	0.164	0.000	0.001	0.000	0.164	0.017	0.000
NiT(2-Me-Pr)[f]	1.900	1.898	0.342	1.859	0.039	0.125	0.114	0.016
NiT(cPr)P	2.073	2.072	0.000	2.069	0.095	0.020	0.020	0.000
NiT(*i*Pr)P	2.085	2.084	0.458	2.029	0.025	0.082	0.096	0.025
NiT(cH)P	2.143	2.141	0.143	2.137	0.003	0.002	0.002	0.006
NiT(1-Et-Pr)P	2.257	2.256	0.000	2.254	0.000	0.000	0.091	0.003
			Reference Compounds					
NiTPP	1.295	1.292	0.256	1.266	0.000	0.000	0.000	0.001
NiOEP tetragonal	1.461	1.461	0.116	1.456	0.000	0.000	0.000	0.000
NiOEP triclinic A	0.087	0.078	0.000	0.000	0.000	0.072	0.031	0.000
NiOEP triclinic B	0.144	0.135	0.000	0.000	0.000	0.066	0.117	0.000
NiP	0.094	0.087	0.013	0.079	0.006	0.033	0.003	0.004

[a] Total out-of-plane deformation (in Å) calculated using all 21 out-of-plane modes. [b] Total out-of-plane deformation (in Å) calculated using the 6 lowest-energy out-of-plane modes. [c] Deformation in the lowest-frequency mode of each symmetry type. [d] Data are taken from the structure of NiT(Pe)P crystallized from dichloromethane by slow diffusion of methanol. Structural parameters are for one of four molecules with similar macrocycle conformations (molecule analyzed contains atom Ni4 and has the least disorder of the pentyl groups). [e] Data are taken from the structure of NiT(Pe)P crystallized by slow evaporation of a solution in piperidine. [f] Data are for one of two molecules with similar macrocycle conformations (molecule analyzed contains Ni1).

Table 3. Energies (in kcal mol^{-1}) of Stable Conformers for Different Alkyl Group Orientations of the Four-Coordinate Low-Spin Nickel(II) Tetra(alkyl)porphyrins Relative to the Lowest Energy $\alpha\beta\alpha\beta$ Conformers

porphyrin	$\alpha\beta\alpha\beta$	$\alpha\alpha\beta\beta$	$\alpha\alpha\alpha\beta$	$\alpha\alpha\alpha\alpha$
NiT(Me)P	0	7.93	*a*	8.14
		Primary Alkyl Groups		
NiT(Et)P	0	6.15	*a*	6.15
NiT(Pr)P	0	6.35	*a*	6.36
NiT(Pe)P	0	6.25	*a*	6.24
		Secondary Alkyl Groups		
NiT(cPr)P	0	7.99	4.44	8.02
NiT(*i*Pr)P	0	13.30	*a*	13.75
NiT(cH)P	0	14.17	*a*	14.85
		Tertiary Alkyl Groups		
NiT(tBu)P	0	21.90	11.87	19.54

[a] No stable conformation was obtained.

Table 4. Out-of-Plane Displacements (in Å) from Normal-Coordinate Structural Decomposition and Selected Structural Parameters for Four-Coordinate Low-Spin Nickel(II) Tetra(alkyl)porphyrin Molecular Mechanics Structures ($\alpha\beta\alpha\beta$ Conformation)

porphyrin	d_{obs}[a]	d_{calc}[b]	B_{2u}[c] d_{sad}	B_{1u}[c] d_{ruf}	Ni–N (Å)	C_α–N–N–C_α (ruffling angle) (deg)	N–C_α–C_m–C_α (π-overlap angle) (deg)
NiT(Me)P	1.892	1.885	0.000	1.885	1.902	39.1	17.9
NiT(Et)P	1.812	1.808	0.000	1.808	1.908	37.4	16.2
NiT(Pr)P	1.799	1.795	0.000	1.795	1.908	37.1	16.0
NiT(Pe)P	1.797	1.793	0.000	1.793	1.908	37.1	16.0
NiT(cPr)P	1.857	1.850	0.000	1.850	1.904	38.3	17.9
NiT(*i*Pr)P	2.245	2.236	0.099	2.233	1.883	46.1	22.3
NiT(cH)P	2.281	2.271	0.102	2.269	1.881	46.8	22.7
NiT(*t*Bu)P	2.764	2.743	0.000	2.743	1.845	56.6	31.2
NiTPP	1.482	1.479	0.005	1.479	1.924	30.7	12.7

[a] Total out-of-plane deformation (in Å) calculated using all 21 out-of-plane modes. [b] Total out-of-plane deformation (in Å) calculated using the 6 lowest-energy out-of-plane modes. [c] Deformation in the lowest-frequency mode of the indicated symmetry type. The $E_g(x)$, $E_g(y)$, A_{1u}, and A_{2u} contributions are 0.000 and are not shown.

$\alpha\alpha\alpha\beta$, $\alpha\alpha\alpha\alpha$, and $\alpha\alpha\beta\beta$, with α and β indicating that the first substituent carbon atom is displaced above or below the mean plane, respectively). Some porphyrins (NiT(Et)P, NiT(Pr)P, and NiT(Pe)P) also possess additional secondary conformers resulting from variations in the orientation of the second carbon of the alkyl substituent. These secondary conformers have nearly the same macrocycle distortions and calculated energies (Tables S2−S4). The energies of the lowest-energy structures for each of the alkyl group orientations ($\alpha\beta\alpha\beta$, $\alpha\alpha\alpha\beta$, $\alpha\alpha\alpha\alpha$, and $\alpha\alpha\beta\beta$) of the low-spin four-coordinate nickel(II) complexes are shown in Table 3, and full details of the calculated energies are given in Table S2 of the Supporting Information. The lowest-energy structures have an $\alpha\beta\alpha\beta$ substituent orientation and a ruffled conformation of the porphyrin macrocycle in agreement with most of the crystallographic data (Table 2). The crystal structures do contain small amounts of other distortions that most likely arise from crystal packing forces, especially packing forces that dictate special substituent orientations. The next higher energy conformer is predicted to be greater than 6 kcal mol^{-1} above the $\alpha\beta\alpha\beta$ conformer, suggesting that these other conformers are inaccessible at ambient temperatures. This is understandable because the $\alpha\beta\alpha\beta$ substituent orientation induces ruffling, which most effectively relieves the peripheral steric repulsions and also contracts the porphyrin core to provide a short and favorable Ni−N bond distance. A more pronounced difference in the energies of the $\alpha\beta\alpha\beta$ and the other conformers is observed for the bulkier substituents.

Table 4 summarizes NSD results for the lowest-energy $\alpha\beta\alpha\beta$ structures (data for other conformations is given in Table S3 of the Supporting Information). The degree of ruffling seen in the MM structures generally increases with the steric bulkiness of the peripheral substituent and varies between approximately 1.8 and 2.7 Å. The ruffling distortion calculated for the Me and primary alkyl porphyrins is somewhat larger than that seen for the hemes in hemeproteins, where the ruffling distortion is seldom more than ∼1.5 Å.[13,23] The minimum energy $\alpha\beta\alpha\beta$ ruffled structures calculated for NiT(Me)P and the porphyrins with primary alkyl substituents (d_{ruf} 1.8−1.9 Å) are similar to the conformations seen crystallographically for NiT(Pe)P and NiT(2-Me-Pr)P (d_{ruf} 1.6−1.9 Å, Table 2). This supports the idea that the nearly planar solid-state crystal structures of NiT(Pr)P (d_{ruf} 0.001 Å) and NiT(Me)P (d_{ruf} 0.000 Å) may be the result of more favorable crystal packing interactions for a nearly planar geometry and that the MM calculated deformations for NiT(Pr)P (d_{ruf} 1.795 Å) and NiT(Me)P (d_{ruf} 1.885 Å) are a more accurate reflection of their solution behavior. Overall, the MM calculations suggest that the degree of ruffling increases in the series Et ≈ Pr ≈ Pe < Me ≈ cPr < *i*Pr ≈ cH < *t*Bu. The predictions that NiT(Me)P is more nonplanar than the porphyrins with primary alkyl groups and that NiT(cPr)P is less nonplanar than the other porphyrins with secondary alkyl substituents are supported by spectroscopic studies in section 2 and arguments based on the steric interactions of these substituents with the porphyrin ring.

Table 4 presents selected structural parameters from the MM calculations, and additional structural parameters are given in Table S4 of the Supporting Information. The MM calculations also accurately predict the porphyrin structural parameters; for example, the Ni−N distances in the porphyrins with secondary alkyl substituents are in the ranges 1.881−1.904 Å (calculated) and 1.888−1.902 Å (crystal), and the C_α−N−N−C_α ruffling angles are 38.3°−46.8° (calculated) and 43.7°−46.2° (crystal). However, the calculations do systematically overestimate the N−C_α−C_m−C_α (π-overlap) torsion angle as noted in an earlier paper.[19]

II. UV−visible Absorption and Resonance Raman Studies of Axial Ligation. A. UV−visible Absorption Spectra. The consequences of the noted structural trends are evident in the optical absorption and vibrational spectra of the porphyrins. The UV−visible absorption spectra of the nickel tetra(alkyl)porphyrins in the noncoordinating solvent dichloromethane are shown in Figure 4. The spectra are similar to those observed previously in CS_2,[18] except for blue shifts of about 10 nm for the B and Q_0 bands and 5 nm for the Q_v band. The latter solvent shifts are likely the result of the differences in the dipole moments of CH_2Cl_2 (dielectric constant 9.08) and CS_2 (2.64). The B and Q bands of the $\pi-\pi^*$ transitions of the porphyrin ring progressively red shift and broaden as the substituent group becomes more bulky. This red shift is usually attributed to nonplanar distortions of the porphyrin macrocycle,[19,23,46,47] although its origin has recently generated some debate in the literature.[19,48−51] Most recently, we completed an exhaustive study of the red shifts in nickel and zinc tetra(alkyl)porphyrins and concluded that nonplanarity of the porphyrin macrocycle was indeed responsible for most of the experimentally observed red shift in nickel tetra(alkyl)porphyrins.[19] Moreover, the spectrum of NiT(cPr)P reported here shows bands approximately at the positions expected on the basis of its degree of ruffling and π-overlap angle, providing further confidence in this conclusion.

Figures 5 and 6 show the absorption spectra obtained in the strongly coordinating solvents pyrrolidine and piperidine, respectively, and the absorption maxima in both coordinating and noncoordinating solvents (taken from Table S5) are plotted in Figure 7. For the less distorted porphyrins with methyl or primary alkyl substituents, there is an approximately 15-nm red shift of the B band for the pyrrolidine complexes (Figure 5) compared to the B band of the four-coordinate species in dichloromethane. A red shift is also observed for the Q_v band (∼40 nm) and the Q_0 band (∼50−60 nm). Previous studies of NiTPP have shown that such shifts are indicative of axial coordination.[14,38,52−55] Similarly, in piperidine the Soret bands for both the four-coordinate and axially ligated species are observed for several of the less nonplanar tetra(alkyl)porphyrins (Figure 6). For the complexes with secondary alkyl groups (NiT(cPr)P, NiT(*i*Pr)P, NiT(cH)P), or tertiary alkyl substituents (NiT(*t*Bu)P), the absorption spectra in pyrrolidine or piperidine are nearly the same as those seen in dichloromethane indicating that the complexes remain four-coordinate. Additional experiments indicated that it is possible to observe the ligated species

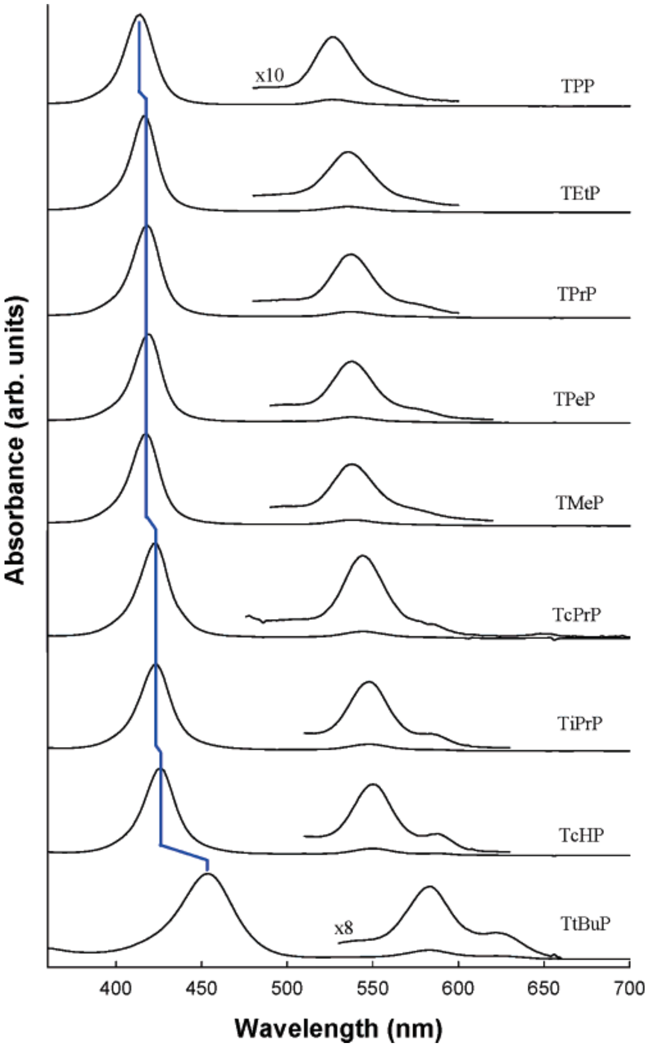

Figure 4. UV−visible absorption spectra for the nickel tetra(alkyl)porphyrins in the noncoordinating solvent dichloromethane.

---

(46) Ravikanth, M.; Chandrashekar, T. K. *Struct. Bond.* **1995**, *82*, 105−188.
(47) Senge, M. In *The Porphyrin Handbook*; Kadish, K. M., Smith, K. M., Guilard, R., Eds.; Academic Press: San Diego, 2000; Vol. 1, pp 239−348.
(48) Dimagno, S. G.; Wertsching, A. K.; Ross, C. R. *J. Am. Chem. Soc.* **1995**, *117*, 8279−8280.
(49) Parusel, A. B. J.; Wondimagegn, T.; Ghosh, A. *J. Am. Chem. Soc.* **2000**, *122*, 6371−6374.
(50) Wertsching, A. K.; Koch, A. S.; DiMagno, S. G. *J. Am. Chem. Soc.* **2001**, *123*, 3932−3939.
(51) Ryeng, H.; Ghosh, A. *J. Am. Chem. Soc.* **2002**, *124*, 8099−8103.
(52) MacCragh, A.; Storm, C. B.; Koski, W. S. *J. Am. Chem. Soc.* **1965**, *87*, 1470−1476.
(53) McLees, D. D.; Caughey, W. S. *Biochemistry* **1968**, *7*, 642−652.
(54) Abraham, R. J.; Swinton, P. F. J. *J. Chem. Soc. B* **1969**, *8*, 903−910.
(55) Walker, F. A.; Hui, E.; Walker, J. M. *J. Am. Chem. Soc.* **1975**, *97*, 2390−2397.

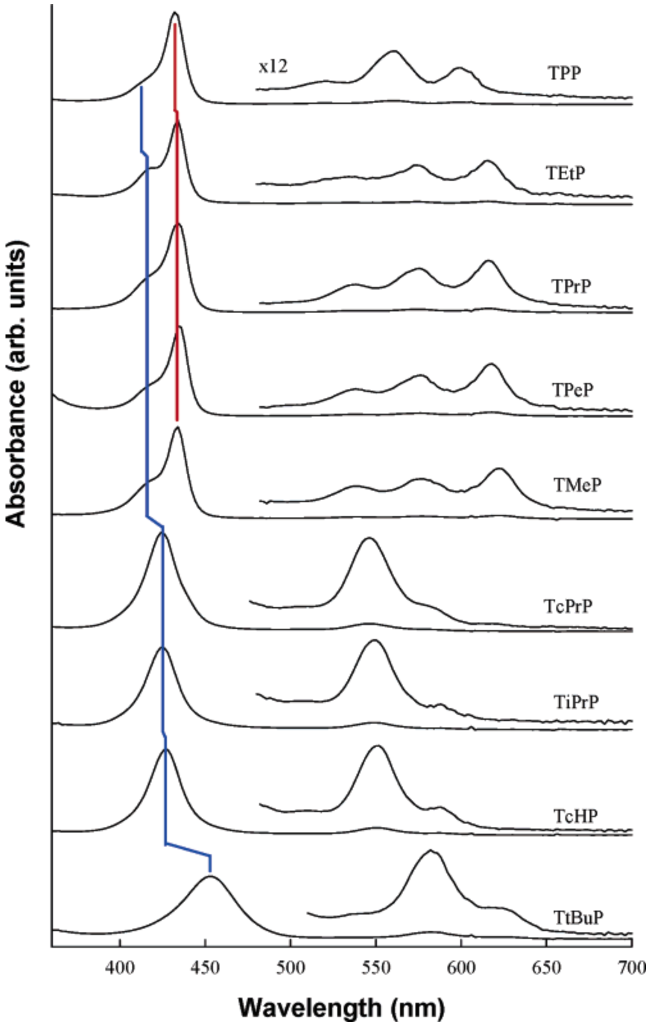

Figure 5. UV−visible absorption spectra for the nickel(II) tetra(alkyl)-porphyrins in the strongly coordinating solvent pyrrolidine. Soret bands for the unligated forms are marked with a blue line, and those for the ligated forms with a red line.

for NiT(cPr)P using the smaller and more basic amine azetidine (see Figure S1).

Based on the peak height ratios for the ligated to unligated species, the amount of the ligated species in piperidine decreases in the order NiT(Et)P (0.70) ≈ NiT(Pr)P (0.72) ≈ NiT(Pe)P (0.67) > NiT(Me)P (0.48). As the data for the more sterically crowded porphyrins indicate that nonplanarity in the four-coordinate low-spin state inhibits binding, the lower concentration of the ligated species seen for NiT(Me)P suggests that this porphyrin is more nonplanar. This finding agrees with the MM calculations (Table 4) which show $d_{\mathrm{ruf}} \approx 1.9$ Å for NiT(Me)P compared to $d_{\mathrm{ruf}} \approx 1.8$ Å for NiT(Et)P, NiT(Pr)P, and NiT-(Pe)P. The fact that NiT(cPr), but not NiT(*i*Pr)P or NiT(cH)P, adds axial ligands in azetidine (see Figure S1) also agrees with the more planar structure calculated for NiT(cPr)P. It is worth noting that a red shift is consistently seen upon axial ligation, even though the switch to the larger high-spin nickel is expected to flatten the macrocycle and therefore produce a blue shift in the optical spectra. In actuality, this blue shift is probably small because the change in ruffling occurs in the flat part of the curve in Figure 7, so the much larger red shift arising from axial ligation and the associated electronic change at the nickel ion is the dominant effect.

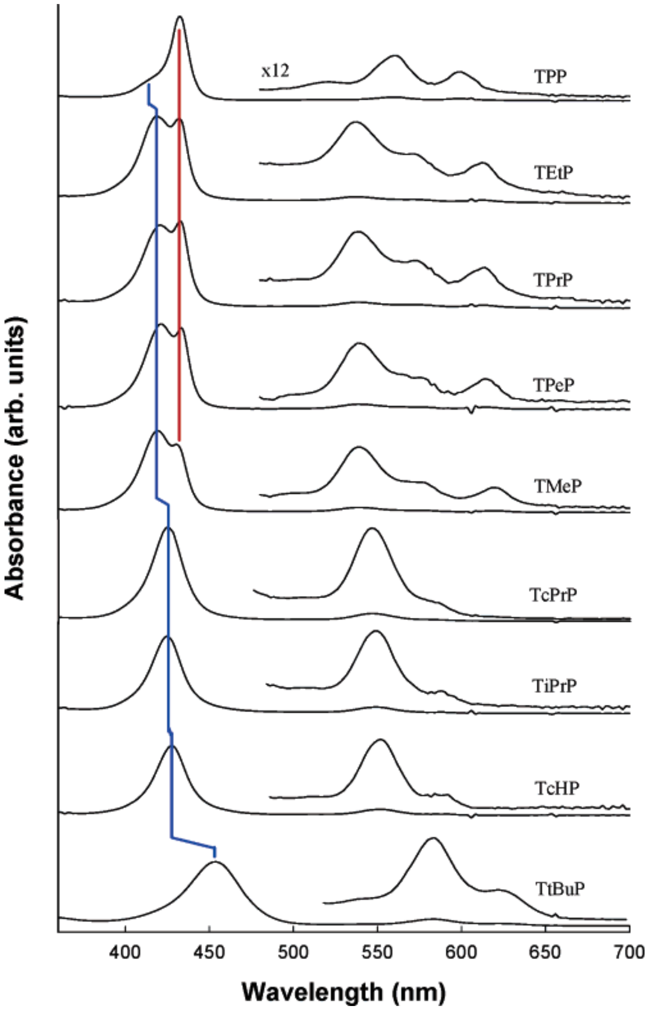

Figure 6. UV−visible absorption spectra for the nickel(II) tetra(alkyl)-porphyrins in the strongly coordinating solvent piperidine. Soret bands for the unligated forms are marked with a blue line, and those for the ligated forms with a red line.

B. Resonance Raman Spectroscopy. The Raman core-size and oxidation-state marker lines, ν_2, ν_3, ν_4, ν_{10}, and ν_{28} are also good structural and ligation state indicators.[18,20,21,25,33,56−59] For example, Soret-excited resonance Raman spectra of the nickel tetra(alkyl)porphyrins in the noncoordinating solvent CS_2 show a decrease in the frequencies of the structure-sensitive lines ν_2, ν_3, ν_4, and ν_{28} due to an increase in nonplanarity caused by bulky *meso* substituents.[18] Some of the spectra in dichloromethane are shown again here as gray lines in Figure 8. A similar decrease in marker line frequencies has been noted in other series of porphyrins with increasing magnitude of nonplanarity,[21] confirming the presence of a negative correlation between frequency and nonplanarity in porphyrins.[23]

Resonance Raman spectra in the high-frequency region (1300−1700 cm^{-1}) for the nickel tetra(alkyl)porphyrins in pyrrolidine are shown in Figure 8. This region contains the well-

---

(56) Shelnutt, J. A.; Majumder, S. A.; Sparks, L. D.; Hobbs, J. D.; Medforth, C. J.; Senge, M. O.; Smith, K. M.; Miura, M.; Luo, L.; Quirke, J. M. E. *J. Raman Spectrosc.* **1992**, *23*, 523−529.

(57) Song, X. Z.; Jentzen, W.; Jia, S. L.; Jaquinod, L.; Nurco, D. J.; Medforth, C. J.; Smith, K. M.; Shelnutt, J. A. *J. Am. Chem. Soc.* **1996**, *118*, 12975−12988.

(58) Kim, D.-H.; Spiro, T. G. *J. Am. Chem. Soc.* **1986**, *108*, 2099−2100.

(59) Kim, D.-H.; Miller, L. A.; Spiro, T. G. *Inorg. Chem.* **1986**, *25*, 2468−2470.

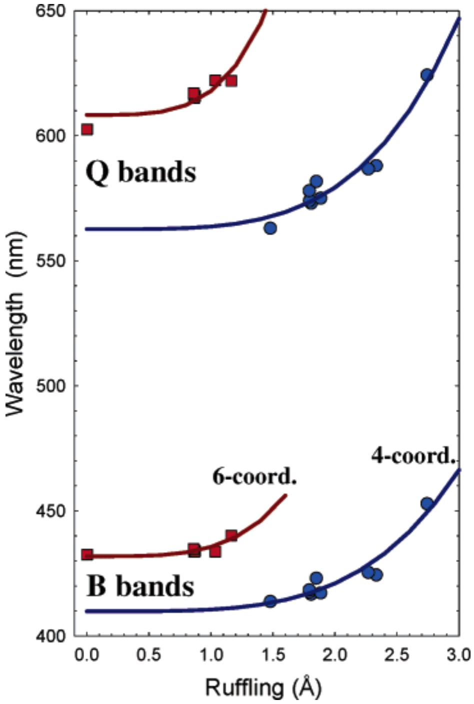

Figure 7. Observed four-coordinate (blue) and six-coordinate (red) absorption maxima (nm) for nickel(II) tetra(alkyl)porphyrins and their pyrrolidine complexes versus ruffling of the corresponding calculated structures. Curve fits are with a homogeneous quartic equation. The azetidine complex is substituted for the NiT(cPr)P pyrrolidine complex, and the reference NiTPP complexes are also included. The data are listed in Table S5 of the Supporting Information.

known structure-sensitive lines, including the oxidation-state marker line ν_4 and the core-size marker lines ν_2 and ν_3.[17,21,60] The ν_2 and ν_4 lines were assigned by analyzing the polarized Raman spectra and the resonance Raman data at different pyrrolidine concentrations as illustrated in Figure 9. Unfortunately, ν_3*, a useful line that is sensitive to nonplanarity and core size, could not be assigned because it is weak and overlies a broad line near 1445 cm^{-1} from the pyrrolidine solvent in the ligated form.

For the highly nonplanar nickel tetra(alkyl)porphyrins, the Raman spectra of the pyrrolidine complexes (black lines) are almost the same as those seen in dichloromethane (gray line). This confirms that these porphyrins do not produce observable amounts of axially ligated species, in agreement with the findings from the UV−visible spectroscopy experiments. On the other hand, for the less distorted methyl and primary alkyl substituted tetra(alkyl)porphyrins, the lines for the ligated species (indicated by the * symbol) dominate the Raman spectra (Figure 8) with excitation at 413.1 nm, a wavelength that is resonant with the B_0 transition of the Soret band of the four-coordinate species. This laser line is also resonant with the B_v transition of the six-coordinate form, and the strength of the spectrum of the six-coordinate species can be explained if the latter resonance is stronger than the B_0 resonance of the four-coordinate complex.

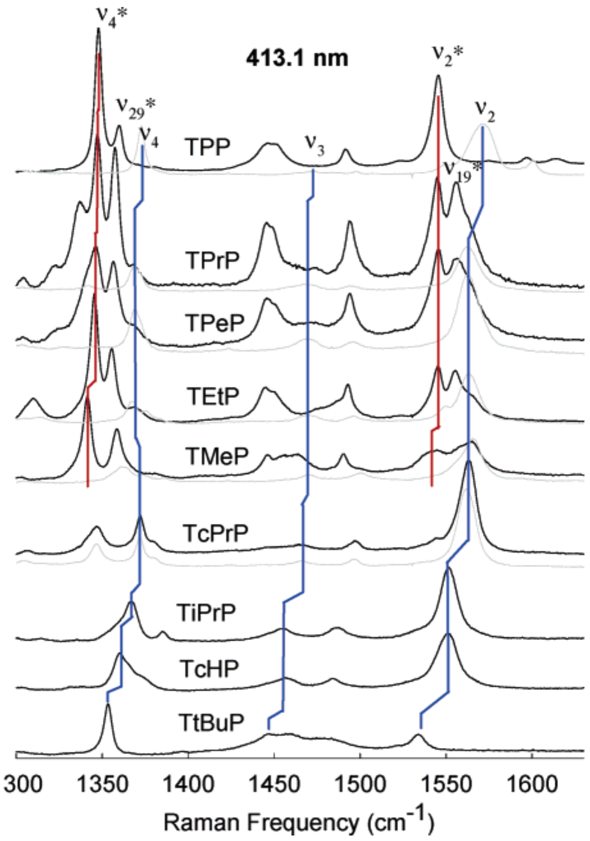

Figure 8. Resonance Raman spectra of nickel(II) tetra(alkyl)porphyrins in pyrrolidine at 413.1 nm excitation (ν_2, ν_4 = four-coordinate form; ν_2*, ν_4* = axially ligated form). Spectra obtained in dichloromethane are shown with gray lines.

The structure-sensitive lines ν_2, ν_4 (Figure 8), and ν_8 (data not shown) downshift by up to ~25 cm^{-1} relative to those of the corresponding porphyrin four-coordinate complexes. (The approximate positions of some vibrations for the four-coordinate complexes are indicated by blue lines in Figures 8 and 9.) The large downshifts in these core-size marker lines are indicative of axial coordination, which induces a change in the electronic configuration of the nickel and expansion of the porphyrin core.[14,58,59,61,62] The axial ligation downshift in the Raman lines corresponds to the large red shift in the absorption bands due to axial ligation.

In a previous paper, we showed that distinct ν_4 lines could be observed for four-, five-, and six-coordinate forms of NiTPP and that the five-coordinate ν_4 is located at an intermediate frequency between the four- and six-coordinate values.[14] Figure 9 shows that only two ν_4 lines are observed in this region during titration with pyrrolidine (i.e., ν_{29}* appears, not a third ν_4* line), indicating that only one ligated species is formed. In addition, ν_{19}*, an inversely polarized structure-sensitive line, appears upon ligation and should not be confused with a line from the five-coordinate species; a similar enhancement of ν_{19}* is observed for NiTPP in coordinating solvent.[14]

C. Experimental Determination of Axial Ligand Binding Affinities and Coordination State. Although the absorption and Raman spectra show that axial ligation goes almost to completion for the Me and primary alkyl porphyrins in pyrrolidine, the coordination number of the ligated species is not conclusively determined by the available spectroscopic data. The coordination number for these porphyrins was investigated by titrating several Ni tetra(alkyl)porphyrins with pyrrolidine in benzene while monitoring the changes in the UV−visible absorption spectrum.[14] Equilibrium constants for axial ligation were then obtained by curve-fitting the changes in the absor-

---

(60) Li, X. Y.; Czernuszewicz, R. S.; Kincaid, J. R.; Su, Y. O.; Spiro, T. G. *J. Phys. Chem.* **1990**, *94*, 31−47.

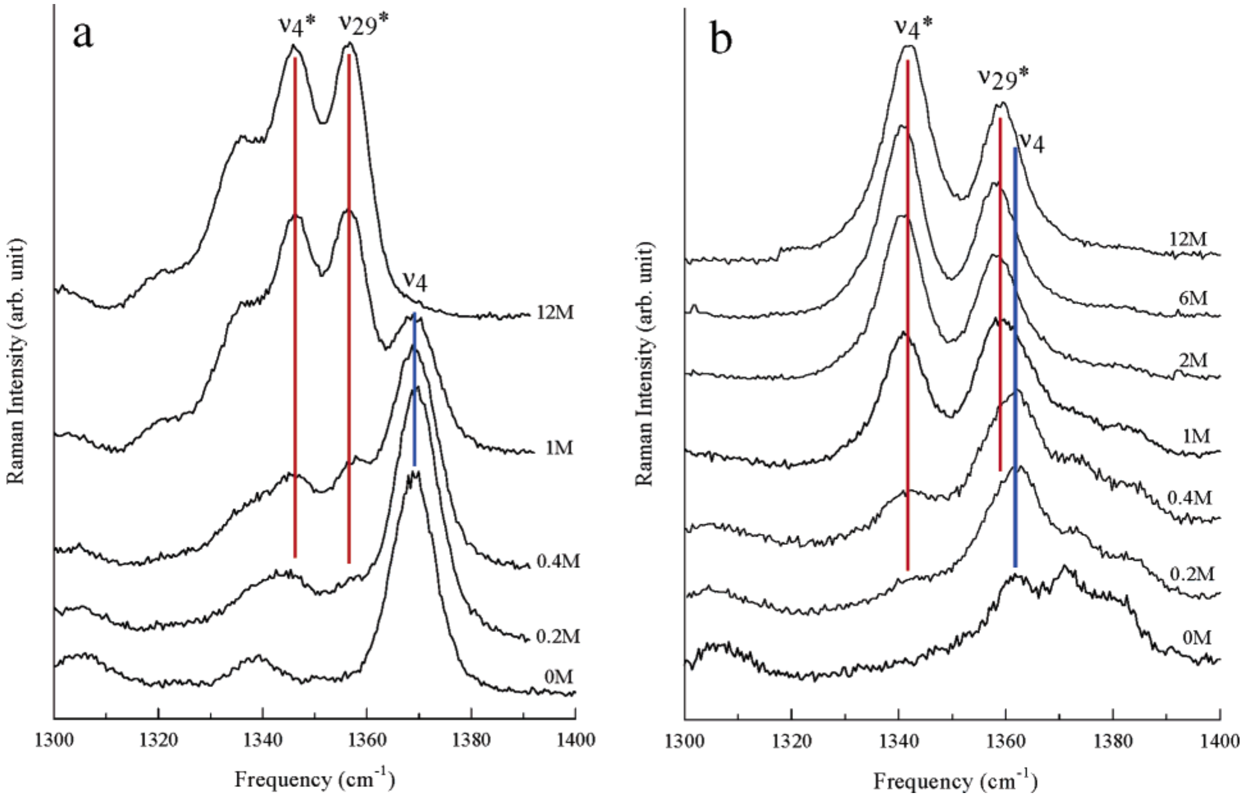

Figure 9. Resonance Raman spectra for (a) NiT(Pr)P and (b) NiT(Me)P in benzene with different pyrrolidine concentrations in the frequency region 1300−1400 cm^{-1} using 413.1 nm excitation.

Table 5. Equilibrium Constants (M^{-1}) for Coordination of Nickel(II) Tetra(alkyl)porphyrins with Pyrrolidine in Benzene and Calculated Ruffling of the Four-Coordinate Low-Spin Structure

porphyrin	K_1	K_2	β^a	d_{ruf} (four-coord)
NiT(Pr)P	4.80×10^{-2}	10.76	0.52	1.795
NiT(Pe)P	1.50×10^{-2}	22.88	0.34	1.793
NiT(Me)P	6.82×10^{-3}	26.63	0.18	1.885
NiTPP[14,63]	2.59	9.49	24.58	0.003−1.479^b

[a] The value for the constant β given in the table is the product of K_1 and K_2, which is approximately equal to β obtained by fitting the titration data with only one equilibrium constant. [b] Multiple stable structures give a range of rufflings.

bance using the successive equilibria described by constants K_1 and K_2 for the addition of the first and second axial ligands or using a single equilibrium constant β (Scheme 1). Details of the titrations and least-squares analysis are given in the Experimental Section and in the Supporting Information. The results obtained from these experiments, along with the data for NiTPP for comparison, are summarized in Table 5. The estimated errors in the values of K_1 and K_2 are approximately 25%, whereas the estimated errors in β are less than 5%.

For the tetra(alkyl)porphyrins which bind pyrrolidine, K_2 varies between 11 and 27 M^{-1}, values which are not too different from that determined for NiTPP (9.5 M^{-1}). In contrast, K_1 is much smaller for the nickel tetra(alkyl)porphyrins (7×10^{-3} to 4.8×10^{-2} M^{-1}) than that seen for NiTPP ($K_1 = 2.6$ M^{-1}). In the case of the nickel tetra(alkyl)porphyrins, an almost identical fit could also be obtained with only one equilibrium constant (β). In contrast, two equilibria were essential to fit satisfactorily the titration data for NiTPP. The ability to fit the titrations for the nickel tetra(alkyl)porphyrins with a single equilibrium constant is possible because K_1 is much less than K_2 for these complexes, which ensures that the concentration of the five-coordinate species is almost negligible.

Because the association constant for the second ligand is much larger than the first, these results indicate that the dominant ligated species is the six-coordinate complex. Based on this equilibrium model, the five-coordinate species reaches a maximum concentration of less than 1% for NiT(Me)P using the determined equilibrium constants. The five-coordinate complex reaches a much higher maximum concentration (10% when the pyrrolidine concentration is about 0.2 M) for NiTPP, where the first and second binding constants are more equal (2.59 and 9.49 M^{-1}).[14] The absence of an appreciable concentration of the five-coordinate nickel complex in the optical spectrum is therefore expected and is also consistent with the lack of lines for a five-coordinate species in the resonance Raman spectra (Figure 9).

The measured value of K_1 is smallest for NiT(Me)P. While the difference in the K_1 values between NiT(Me)P and NiT(Pr)P or NiT(Pe)P is small and close to the error in the measurements, it is worth noting that there appears to be an inverse relationship between K_1 and the degree of macrocycle nonplanarity. The smaller value of K_1 seen for NiT(Me)P is consistent with the more nonplanar structure calculated for this porphyrin compared to NiT(Pr)P or NiT(Pe)P.

III. Computational Studies of the Axially Ligated Nickel Tetra(alkyl)porphyrins. A. Conformations of the Axially Ligated Complexes. For comparison with the following molecular mechanics results, Table 6 summarizes X-ray crystal data for six-coordinate high-spin and four-coordinate low-spin complexes. Axial ligation and the associated switch to high-spin nickel(II) significantly increases the Ni−N$_{\text{pyrrole}}$ distance (by about 0.12 Å or 6%) as an electron goes into the $d_{x^2-y^2}$

Table 6. Comparisons of the Crystal Structures of Low-Spin and Six-Coordinate High-Spin Nickel Porphyrin Complexes

	Ni–N_{pyr}	total distortion		B_{2u}[c]	B_{1u}	A_{2u}	$E_g(x)$	$E_g(y)$	A_{1u}
porphyrin	(Å)	d_{obs}[a]	d_{calc}[b]	d_{sad}	d_{ruf}	d_{dom}	$d_{wav(x)}$	$d_{wav(y)}$	d_{pro}
NiTPP	1.931	1.295	1.292	0.256	1.266	0.000	0.000	0.000	0.001
NiTPP $(pip)_2$	2.043	0.341	0.259	0.000	0.000	0.000	0.144	0.215	0.000
NiTPP $(1\text{-Me-Im})_2$	2.052	0.362	0.314	0.000	0.000	0.000	0.118	0.292	0.000
$NiBr_4(CN)_4TPP$	1.919	3.080	3.077	3.068	0.205	0.090	0.050	0.017	0.034
$NiBr_4(CN)_4TPP\ (py)_2$	2.056	1.951	1.937	1.867	0.489	0.000	0.073	0.142	0.034
NiOETNP (molecule 1)	1.917	3.313	3.310	3.250	0.632	0.011	0.091	0.048	0.041
NiOETNP (molecule 2)	1.921	3.010	3.009	2.877	0.874	0.064	0.042	0.055	0.077
NiOETNP $(py)_2$	2.049	2.483	2.460	2.306	0.844	0.052	0.124	0.054	0.058

[a] Total out-of-plane deformation (in Å) calculated using all 21 out-of-plane modes. [b] Total out-of-plane deformation (in Å) calculated using the 6 lowest-energy out-of-plane modes. [c] Deformation in the lowest-frequency mode of each symmetry type.

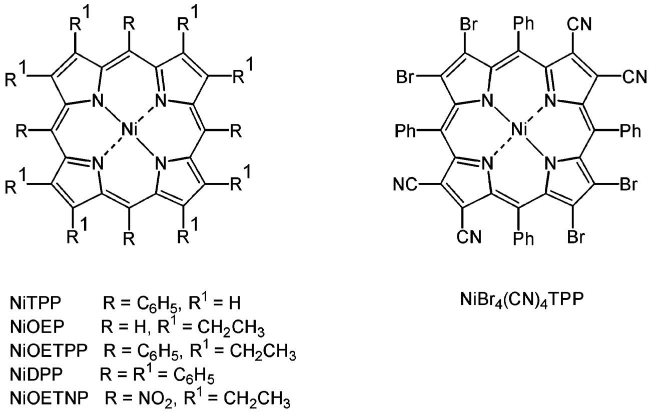

Figure 10. Structures of nickel(II) porphyrins, including those with known crystal structures of the six-coordinate form.

orbital. The replacement of the small low-spin nickel atom with the much larger high-spin nickel atom flattens nonplanar porphyrin macrocycles. For example, the crystal structure of NiTPP is moderately ruffled[64] but becomes nearly planar upon complexation with nitrogenous base ligands such as piperidine or 1-methyl-imidazole.[14,65] Sterically crowded nickel(II) 2,3,12,13-tetrabromo-7,8,17,18-tetracyano-5,10,15,20-tetraphenylporphyrin ($NiBr_4(CN)_4TPP$, Figure 10) is very saddled but flattens upon ligation with pyridine[16] as does 2,3,7,8,12,13,17,18-octaethyl-5,10,15,20-tetranitroporphyrin (OETNP).[15]

MM calculations for the four-coordinate high-spin and six-coordinate high-spin nickel tetra(alkyl)porphyrins (Table 7) indicate that the $\alpha\beta\alpha\beta$ ruffled structure is still the lowest energy conformation. However, compared to the low-spin complexes there are now smaller energy differences between the conformations. This suggests that additional macrocycle conformations are accessible in solution at room temperature for the high-spin ligated complexes. This can be understood by considering the relationship between conformation and core size; the $\alpha\beta\alpha\beta$ ruffled conformation produces a small core size, whereas larger core sizes are obtained from the out-of-plane deformations produced with other substituent orientations.[20] The conformations resulting from the latter substituent orientations are more compatible with the larger nickel ion (longer equilibrium Ni−$N_{pyrrole}$ distance used in the MM force field) of the high-spin and axially ligated complexes. Hence, the switch to high-spin nickel alters the conformational energy landscape by destabilizing the ruffled conformation and stabilizing the other conformations. Full details of the calculated energies for the high-spin four-coordinate complexes (analogous to the photoexcited Ni(d,d) state), high-spin five-coordinate (mono-pyrrolidine) complexes, and high-spin six-coordinate (bis-pyrrolidine) complexes of the nickel tetra(alkyl)porphyrins are provided in Tables S7−S9 of the Supporting Information. It is important to bear in mind that the MM energies are conformational energies and omit the electronic energy of ligand binding and the entropic contributions to the free energy; thus they address only the conformational aspects of the energetics of complexation. Predictions based on these energies assume that other contributions are equal for a particular axial ligand.

Table 7. Energies (in kcal mol^{-1}) for Different Alkyl Group Orientations of the High-Spin Nickel(II) Tetra(alkyl)porphyrins Relative to the Lowest Energy $\alpha\beta\alpha\beta$ Conformer

porphyrin		$\alpha\beta\alpha\beta$	$\alpha\alpha\beta\beta$	$\alpha\alpha\alpha\beta$	$\alpha\alpha\alpha\alpha$
NiT(Me)P	four-coordinate (d,d excited state)	0	1.30	0.83	1.18
	six-coordinate (bis-pyrrolidine)	0^a	1.48^b	1.11^b	1.38^b
NiT(Et)P	4-coordinate	0	1.18	0.74	1.07
	6-coordinate	0^a	0.51^b	0.34^b	0.52^b
NiT(Pr)P	four-coordinate	0	1.30	0.83	1.18
	six-coordinate	0^a	0.57^b	0.40^b	0.59^b
NiT(Pe)P	four-coordinate	0	1.27	0.80	1.14
	six-coordinate	0^a	0.54^b	0.48^b	0.56^b
NiT(cPr)P	four-coordinate	0	2.44	1.50	1.70
	six-coordinate	0^a	2.51^b	1.79^a	2.09^b
NiT(*i*Pr)P	four-coordinate	0	4.83	*d*	4.08
	six-coordinate	0^a	6.81^c	*d*	4.27^b
NiT(cH)P	four-coordinate	0	5.36	*d*	4.48
	six-coordinate	0^a	4.67^b	*d*	5.06^b
NiT(*t*Bu)P	four-coordinate	0	8.80	3.32	2.03
	six-coordinate	0^a	8.01^a	2.62^a	3.66^b

[a] With the N−H bonds of the ligands sitting between the M−$N_{pyrrole}$ bonds and the mean planes of the axial ligands perpendicular to each other. [b] With the N−H bonds of the ligands sitting along the Ni−$N_{pyrrole}$ bonds and the mean planes of the axial ligands perpendicular to each other. [c] With the N−H bonds of the ligands sitting along the Ni−$N_{pyrrole}$ bonds and the mean planes of the axial ligands parallel to each other. [d] No stable conformation observed.

NSD analyses of the $\alpha\beta\alpha\beta$ four-coordinate high-spin and six-coordinate high-spin structures are summarized in Table S16 of the Supporting Information, with a complete listing in Tables S10−S12. Selected structural parameters are provided in Tables S13−S15. The Ni−$N_{pyrrole}$ distances for the high-spin four-coordinate complexes (1.966−2.028 Å) are much longer than those seen for the low-spin complexes (1.845−1.908 Å)

---

(61) Shelnutt, J. A.; Alston, K.; Ho, J. Y.; Yu, N. T.; Yamamoto, T.; Rifkind, J. M. *Biochemistry* **1986**, *25*, 620−627.
(62) Shelnutt, J. A. *J. Am. Chem. Soc.* **1987**, *109*, 4169−4173.
(63) Jentzen, W.; Unger, E.; Song, X. Z.; Jia, S. L.; TurowskaTyrk, I.; SchweitzerStenner, R.; Dreybrodt, W.; Scheidt, W. R.; Shelnutt, J. A. *J. Phys. Chem. A* **1997**, *101*, 5789−5798.
(64) Maclean, A. L.; Foran, G. J.; Kennedy, B. J.; Turner, P.; Hambley, T. W. *Aust. J. Chem.* **1996**, *49*, 1273−1278.
(65) Kirner, J. F.; Garofalo, J., Jr.; Scheidt, W. R. *Inorg. Nucl. Chem. Lett.* **1975**, *11*, 107−112.

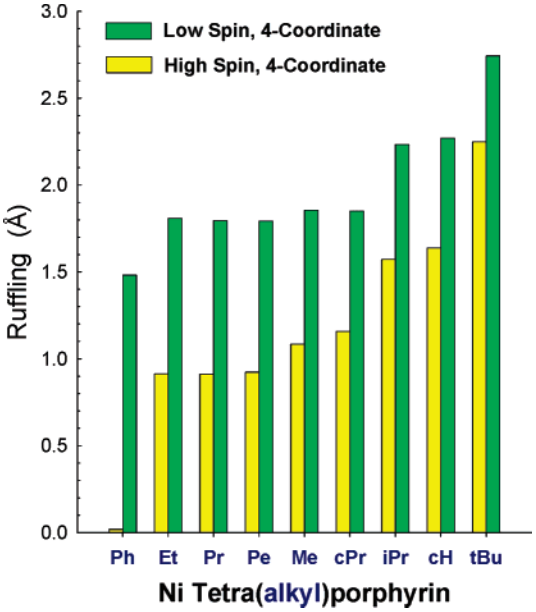

Figure 11. Ruffling deformations (in Å) for the nickel tetra(alkyl)-porphyrins from the NSD analysis of the low-spin (green) and high-spin (yellow) four-coordinate MM structures.

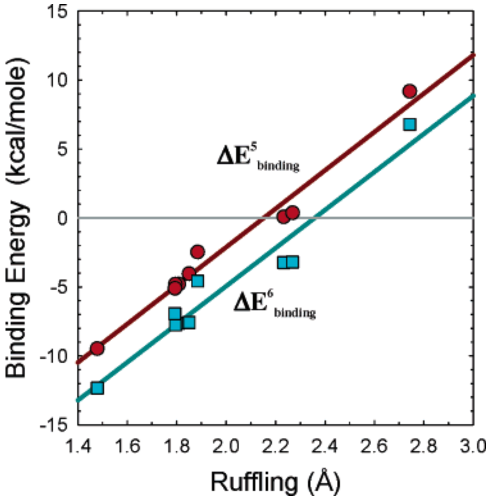

Figure 12. Calculated conformational binding energies for nickel(II) tetra-(alkyl)porphyrins for the five- ($\Delta E^5_{\text{binding}}$) and six- ($\Delta E^6_{\text{binding}}$) coordinate complexes with pyrrolidine versus ruffling of the four-coordinate form. $\Delta E^5_{\text{binding}} = E^{\alpha\beta\alpha\beta}_{5c} - (E^{\alpha\beta\alpha\beta}_{4c} + E_{\text{pyrrolidine}})$; $\Delta E^6_{\text{binding}} = E^{\alpha\beta\alpha\beta}_{6c} - (E^{\alpha\beta\alpha\beta}_{4c} + 2 \times E_{\text{pyrrolidine}})$. $E_{\text{pyrrolidine}} = 9.97$ kcal mol^{-1}.

consistent with the significantly longer equilibrium Ni$-$N$_{\text{pyrrole}}$ distance used in the force field. The Ni$-$N$_{\text{pyrrole}}$ distances increase a little further upon ligation to form the six-coordinate complex (1.982$-$2.031 Å). Concomitant with the changes in the Ni$-$N$_{\text{pyrrole}}$ distances there are decreases in macrocycle ruffling, with d_{ruf} going from 1.79 to 2.74 Å (four-coordinate low-spin) to 0.91$-$2.25 Å (four-coordinate high-spin) to 0.86$-$1.82 Å (six-coordinate high-spin). Small amounts of the other nonplanar deformation modes are also seen in the axially ligated complexes (Table S16) most likely due to the asymmetry of the axial ligands and/or the asymmetry induced by the orientations of the ligands. The similarity in the structures of the six- and four-coordinate high-spin complexes suggests that direct interaction between the axial ligand and the substituent groups is a minor effect, with the possible exception of the *tert*-butyl substituents.

As illustrated in Figure 11, the percentage decrease in ruffling upon switching from low- to high-spin four-coordinate nickel varies markedly with the alkyl substituent: for methyl and primary alkyl substituents, the decrease in ruffling is 42$-$49%; for secondary alkyl groups, 28$-$37%; for the *tert*-butyl group, 18%. For reference, the NiTPP goes almost completely planar for the high-spin four-coordinate complex (99% decrease in ruffling). The smaller changes apparent for the bulkier alkyl groups are consistent with the approximately quadratic dependence of the energy required to deform the porphyrin macrocycle,[17] reminiscent of the nonlinear dependence of electronic transition energies on the ruffling deformations (Figure 7). For the porphyrins with methyl or primary alkyl substituents, the energy (caused by the change in the equilibrium Ni$-$N bond distance for low- and high-spin Ni) that is required to cause a large change in nonplanar deformation is small because the structures are on the shallow portion of the potential energy surface. In contrast, the porphyrins with secondary and tertiary substituents are located on the steeper portion of the potential energy curve, and thus only smaller amounts of flattening can be induced by the switch to high-spin nickel(II).

B. Conformational Contributions to Ligand Binding Energies. The energies obtained from the MM calculations were used to estimate the conformational part of the ligand binding energies. Approximate binding energies for the addition of pyrrolidine were calculated by subtracting the energy of the pyrrolidine ligand(s) and the lowest-energy four-coordinate conformer from the energies of the five- or six-coordinate pyrrolidine complexes (Figure 12 and Table S6). These binding energies are only the structural contribution to the binding free energy, omitting entropic and electronic enthalpic contributions associated with ligand binding. In particular, the entropic component associated with bringing together two or three molecules at room temperature is not included in the calculations and will likely shift the calculated binding energies to more positive (less favorable) values. Nonetheless, the binding energies do provide an estimate of the trend in enthalpic preference of these distorted porphyrins for binding axial ligands. The MM calculations correctly reproduce the trends seen in the spectroscopic studies in section II (Figure 12). Negative binding energies are typically obtained for the methyl and primary alkyl substituted porphyrins and the reference compound NiTPP. The binding energies become more positive for the porphyrins containing secondary or tertiary alkyl substituents, such that the binding energy calculated for NiT(tBu)P is large and ligand binding is strongly disfavored.

The MM calculations also underscore the fact that the major effect causing the observed decrease in ligand binding affinity with increased ruffling is the required increase in core size due to the switch from low-spin to high-spin nickel (see Table S6). The energy increase from low- to high-spin four-coordinate nickel is small (0.56 kcal mol^{-1}) for NiT(Me)P but large (13.56 kcal mol^{-1}) for NiT(tBu)P. This energy increase is related to the inability of the porphyrin to flatten and the core to expand to accommodate the large Ni$-$N bond of high-spin Ni for the more ruffled porphyrins. As we observed above, for the bulkier substituents, the macrocycle cannot flatten enough to allow the core to expand sufficiently to accept the larger Ni ion (Figure 11). The energy decreases associated with the addition of pyrrolidine ligands to the high-spin complexes are similar for

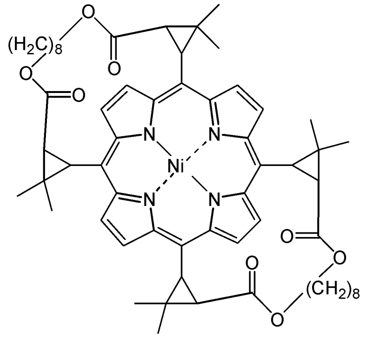

NiBCP-8

Figure 13. Structure of the bridled chiroporphyrin NiBCP-8.

both porphyrins: −3.03 kcal mol^{-1} (five-coordinate) and −2.10 kcal mol^{-1} (six-coordinate) for NiT(Me)P, compared to −4.38 and −2.40 kcal mol^{-1} for NiT(*t*Bu)P, respectively (see Table S6 of the Supporting Information).

IV. Implications and Potential Uses of the Ligation-Induced Structural Changes. Resonance Raman and UV−visible spectroscopy, together with X-ray structures, molecular mechanics calculations, and normal-coordinate structural decomposition analysis, indicate that the axial ligand affinity within the series of nickel(II) tetra(alkyl)porphyrins depends strongly on the degree of macrocycle ruffling, which is in turn determined by the bulkiness of the *meso* substituents. Specifically, the ligand affinity decreases markedly as the alkyl group becomes larger and the amount of ruffling in the four-coordinate form increases. MM calculations show that this decrease in ligand affinity is related to how readily the substituents permit the ring to flatten to accommodate the high-spin nickel ion and not to direct steric inhibition of ligand binding by the substituents. These findings agree with previous anecdotal evidence suggesting that peripherally crowded and very nonplanar nickel porphyrins (e.g., NiDPP and NiOETPP, Figure 12) tend not to bind axial ligands under conditions where nominally planar porphyrins with similar substituent electronic effects (e.g., NiOEP and NiTPP) do bind ligands.[21,44,66] Axial ligand binding has been observed in very nonplanar porphyrins but only when electron-withdrawing substituents are present, e.g., for NiOETNP[15] and NiBr$_4$(CN)$_4$-TPP.[16]

Spectroscopic titration studies show that the decrease in axial ligand affinity occurs primarily because of a large decrease in the binding affinity for the first ligand which induces the nickel spin-state change and flattening of the porphyrin ring. The decrease in the first axial ligand binding affinity compared to NiTPP is large (10^{-2} to 10^{-3}) even for porphyrins with methyl or primary alkyl substituents. When binding the second axial ligand, only a small portion of the energy of ligand binding goes into additional small structural changes, so the net binding energy is much higher, giving binding constants for the methyl or primary alkyl substituted porphyrins that are similar to those seen for Ni porphyrins for which nearly planar conformers are accessible at room temperature (e.g., NiTPP and NiOEP). In contrast, for very bulky substituents such as *tert*-butyl, accessing high-spin nickel is energetically prohibitive and this effectively inhibits axial ligation.

The relationship between porphyrin distortion and axial ligand affinity may have implications for methyl-coenzyme M reductase and, more generally, for the many hemeproteins and photosynthetic proteins which have their hemes and photosynthetic pigments in moderately nonplanar conformations maintained by the surrounding protein.[22−24] Nonplanar deformations are known to alter many biologically relevant properties such as redox potentials, electron-transfer rates, and photophysical processes.[23,46,47,67] The present study indicates that nonplanar deformations, in this case maintained by the *meso* alkyl substituents rather than by a protein matrix, also have an impact on axial ligation. Specifically, holding the tetrapyrrole macrocycle in a moderately nonplanar geometry provides a mechanism for adjusting the ligand affinity and, in particular, modulating the relative affinities of the fifth and sixth ligands. Although the nickel porphyrin studies are not directly applicable to axial ligation by iron porphyrins, they do suggest specific structural mechanisms that may influence the more complex electronic interactions involved in axial ligand binding to heme. In fact, it would not be surprising to find that nonplanar deformations also influence the axial coordination behavior of heme, especially given that investigations of strapped porphyrins[68,69] imply that nonplanar heme distortion might provide a mechanism for differentiating CO and O$_2$ binding, and a change in ruffling of the heme has been suggested as a mechanism for regulating NO affinity and reactivity in nitrophorins (NO-transport proteins).[70]

Expansion of the nickel ion, either by axial ligation or by formation of the photoexcited Ni (*d,d*) state, causes a significant change in the relative energies of the porphyrin conformations (α*β*α*β*, αα*ββ*, ααα*β*, and αααα). While an α*β*α*β* (ruffled) conformer is strongly favored for the low-spin four-coordinate species, the MM calculations indicate a narrowing of the energy differences between the conformers when the nickel ion is expanded. This finding is consistent with a previous study on the Ni(d,d) excited state of NiT(*t*Bu)P with time-resolved absorption spectroscopy, which indicated a transient switch from the α*β*α*β* ground-state conformer to a different conformer in the excited high-spin state (unligated) complex. The conformer in the excited (d,d) state is most likely the ααα*β* conformer,[44] which is almost as effective as the αααα conformation in allowing core expansion because it admits a variable amount of the doming deformation that favors a large core. The suggestion[44] of a conformational switch was based in part on the observation that the excited state lifetime was extraordinarily long and showed an dependence on temperature and the solvent dielectric properties, indicating a kinetic barrier to recovery of the low-spin ground-state conformation and the presence of a dipole moment for the excited state. The latter is inconsistent

---

(66) Retsek, J. L.; Drain, C. M.; Kirmaier, C.; Nurco, D. J.; Medforth, C. J.; Smith, K. M.; Chirvony, V. S.; Fajer, J.; Holten, D. *J. Am. Chem. Soc.* **2003**, *125*, 9787−9800.

(67) Recent investigations of the large red shifts seen in the optical spectra of peripherally crowded nonplanar porphyrins have led some research groups (Wertsching, A. K.; Koch, A. S.; DiMagno, S. G. *J. Am. Chem. Soc.* **2001**, *123*, 3932−3939. Ryeng, H.; Ghosh, A. *J. Am. Chem. Soc.* **2002**, *124*, 8099−8103) to propose that the observed shifts (and by implication the changes seen in other properties) are simply the result of substituent effects. A recent paper by our group[19] confirms that the large red shifts seen in peripherally crowded nonplanar porphyrins are indeed caused by nonplanar deformation and shows that the attribution of the red shifts to substituent effects resulted from the use of inappropriate model structures in the earlier calculations.

(68) Desbois, A.; Momenteau, M.; Lutz, M. *Inorg. Chem.* **1989**, *28*, 825−834.

(69) David, S.; James, B. R.; Dolphin, D.; Traylor, T. G.; Lopez, M. A. *J. Am. Chem. Soc.* **1994**, *116*, 6−14.

(70) Roberts, S. A.; Weichsel, A.; Qiu, Y.; Shelnutt, J. A.; Walker, F. A.; Montfort, W. R. *Biochemistry* **2001**, *40*, 11327−11337.

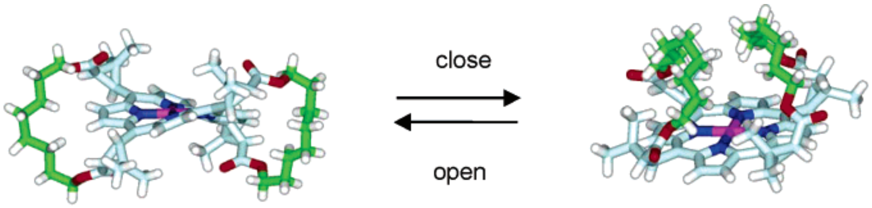

Figure 14. Open (left) and closed (right) forms of prototype nanotweezers based on the bridled chiroporphyrin BCP-8.[10] The structures were generated using published crystallographic data for the low-spin nickel(II) complex (left) and the zinc(II) complex (right) of BCP-8.

with an $\alpha\beta\alpha\beta$ ruffled conformation for the excited state, but a doming contribution to the distortion allows a *z*-dipole moment, which could interact with the polar solvents.

The significant conformational change resulting from the expansion or contraction of the nickel ion may also provide a novel method for initiating large-scale structural alterations for use in molecular devices. We are currently examining the potential of nickel tetra(alkyl)porphyrins as molecular machines using the bridled chiroporphyrin BCP-8 (Figure 13) as a molecular nanotweezer.[10] Crystallographic data[10] show that the low-spin nickel(II) complex NiBCP-8 displays an $\alpha\beta\alpha\beta$ ruffled conformation of the porphyrin macrocycle (Figure 14, left), the same conformation seen for the low-spin nickel tetra(alkyl)porphyrins. In contrast, the complex with the larger zinc(II) ion has an $\alpha\alpha\alpha\alpha$ orientation of the substituents, a much more planar macrocycle, and the straps on the same face of the porphyrin and folded together like a pair of tweezers (Figure 14, right). Given that high-spin nickel(II) is also a large ion (it is the same size as Zn(II) in our force field),[12] it is reasonable to suppose that high-spin NiBCP-8 would behave like the zinc(II) complex. In other words, addition of axial ligands or absorption of a photon will actuate and close the NiBCP-8 nanotweezers.

MM calculations of low- and high-spin NiBCP-8 show two key driving forces for this remarkable conformational change: the previously discussed expansion of the metal and the effect of the short straps in destabilizing the $\alpha\beta\alpha\beta$ ruffled conformer. Spectroscopic studies also show that axial ligands (e.g., azetidine) can bind and switch the nickel spin state, presumably because the cyclopropyl groups at the *meso* positions are not so bulky that they prevent axial ligation. Clearly, the present studies show that there is a trade off between providing the large distortion and large barriers to interconversion between conformers, which are desirable for an effective molecular machine, and ensuring the ability to switch the machine between conformers by using axial ligation or a photoinduced excitation to actuate the nanodevice. The present study suggests that molecular mechanics calculations may aid in designing nanodevices with appropriate conformations and switching characteristics. Detailed studies of the NiBCP-8 nanotweezers will be reported shortly.

Acknowledgment. This work was supported by the Division of Materials Sciences and Engineering, Office of Basic Energy Sciences, U.S. Department of Energy and the Division of Chemical Sciences, Geosciences and Biosciences, Office of Basic Energy Sciences, U.S. Department of Energy (DE-FG03-02ER15369). Sandia is a multiprogram laboratory operated by Sandia Corporation, a Lockheed-Martin company, for the United States Department of Energy under Contract DE-ACO4-94AL85000. This work was partially supported by a grant from the National Science Foundation (CHE-99-04076) (K.M.S.) and by the Ministère de la Recherche of France under the program “Recherche Technologique de Base dans le Domaine des Micro et Nanotechnologies ” (Grant “Post-CMOS Moléculaire 200 mm”).

Supporting Information Available: Calculated energies (Tables S2, S7−9), NSD analyses (Tables S3, S10−12), selected structural parameters (Tables S4 and S13−S15) for low-spin four-coordinate, high-spin four-coordinate, five-coordinate (monopyrrolidine), and high-spin six-coordinate (bis-pyrrolidine) complexes of the nickel tetra(alkyl)porphyrins, and NSD displacements for the four- and six-coordinate $\alpha\beta\alpha\beta$ conformers of the high-spin nickel(II) tetra(alkyl)porphyrins (Table S16). Tables of absorption maxima (S5) and calculated binding energies and energy differences (S6). This material is available free of charge via the Internet at http://pubs.acs.org.

JA045309N